Tectonic Geomorphology and Late Quaternary Deformation on the Ragged Mountain Fault, Yakutat Microplate, South Coastal Alaska

J.P. McCalpin[1],F. Gutierrez[2], R.L. Bruhn[3], J. Guerrero[2], T.L. Pavlis[4], and P. Lucha[5]

[1] GEO-HAZ Consulting, Inc., Crestone, CO, USA.

[2] Department of Earth Sciences, University of Zaragoza, SPAIN.

[3] Independent geologist, Hansville, Washington, USA.

[4] Department of Geological Sciences, University of Texas-El Paso, USA.

[5] Department of Humanities and Education, University of Zaragoza, SPAIN

Correspondingauthor: James McCalpin (mccalpin@geohaz.com)

Keywords: paleoseismology, tectonic geomorphology, trenching, Yakutat Terrane

Abstract

The 33 km-long Ragged Mountain fault (RMF) forms the northwestern corner of the Yakutat Terrane, which is colliding with the North American plate in south coastal Alaska at ~5.5 cm/yr. The fault zone contains three types of scarps in a zone up to 175 m wide: (1) antislope scarps on the lower range front, (2) a sinuous thrust scarp at the toe of the range front, and (3) a swarm of flexural-slip scarps on the footwall. Trenches across the first two scarp types reveal evidence for two Holocene surface ruptures, plus several late Pleistocene ruptures. In the antislope scarp trench, ruptures occurred at 0.5-3.9 ka; slightly younger than 8.3 ka; and at 18.1-21.8 ka (recurrence intervals 4.4-8 kyr and 9.8-13.3 kyr). Displacements per event ranged from 15 to 40 cm. In the thrust trench ruptures are dated at 2.8-5.9 ka; 5.9-17.2 ka, and 17.2-44.9 ka (mean recurrence intervals 7.2 kyr and 19.5 kyr). Displacements per event ranged from 26-77 cm. We interpret the thrust fault as the primary seismogenic structure, and its largest trench displacement (77 cm) equates to the average displacement expected for a 33 km-long reverse rupture. The flexural-slip scarp, in contrast, was rapidly formed ca. 4 ka but its sag pond sediments have continued to slowly fold up to present. The southern third of the fault is dominated by large gravitational failures of the range front (as large as 2.5 km wide, 0.6-0.7 km long, and 200-250 m thick), which head in a linear, 40 m-deep range-crest trough filled with lakes, a classic expression of deep-seated gravitational slope deformation.

1 Introduction

The Saint Elias orogen of southern Alaska and the Yukon, Canada is an actively deforming belt of mountains created by collision and subduction of the Yakutat microplate, a former oceanic plateau and subduction complex (Fig. 1; Plafker, 1987; Chapman et al., 2008). With a convergence rate of ~5.5 cm/yr, the orogen has formed some of the most extreme tectonic geomorphology on the planet. In the western orogen (south coastal Alaska)the microplate is marked by moderate-relief mountain blocks that rise above a broad, glaciated lowland. The northwest corner of the microplate is formed by the N-S trending, 33 km-long Ragged Mountain fault (RMF; Fig. 2), which juxtaposes the younger Yakutat Terrane against the Early Tertiary plate margin (Prince William Terrane).

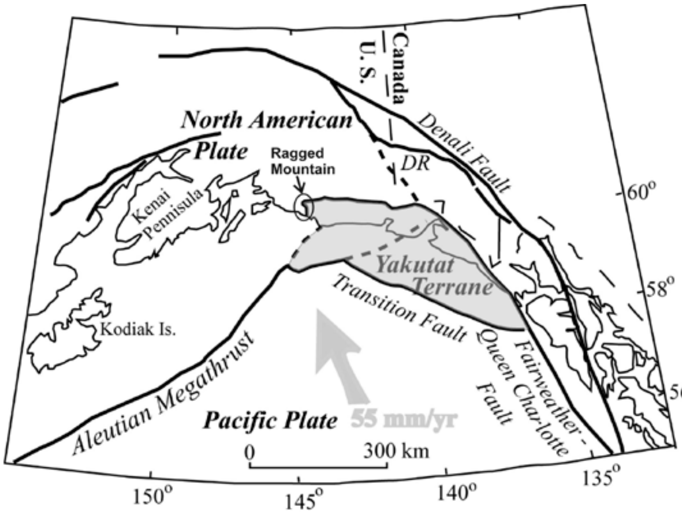

Figure 1. Plate tectonic setting of the Yakutat Terrane (gray) and the Ragged Mountain fault at its northwest corner (after Bruhn et al., 2004).

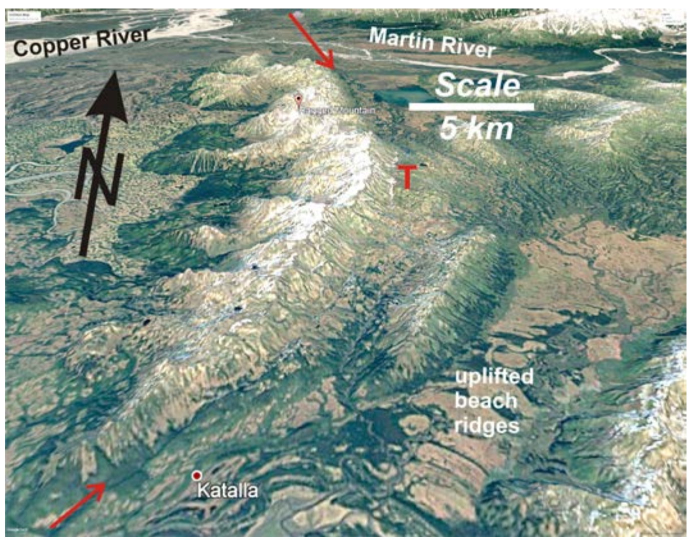

Fig. 2. Satellite view of Ragged Mountain and the RMF (between red arrows) at the base of its eastern range front. The range-front trough described by Tysdal et al. (1976b) is the narrow snow-filled lineament immediately left of the red “T”.

In the 1950s Kachadoorian (1956) noticed fresh-looking 9 m-high fault scarps on the RMF and inferred it was an active fault. However, the kinematics of the fault pose a major enigma for paleoseismologists. Structurally, Paleogene rocks of the Prince William Terrane have been thrust eastward over the Tertiary-age Stillwater Formation of the Yakutat Terrane. The fault trace is expressed mainly by a narrow belt of antislope scarps and grabens related to normal faults that offset late Pleistocene and Holocene deposits (talus, rock avalanches). This conspicuous evidence of young extensional deformation led Tysdal et al. (1976) to infer that the upper plate of the low-angle (8°) RMF has experienced a reverse gravity-driven back-sliding towards the Copper River of more than 180 m in Holocene times (Fig. 3).

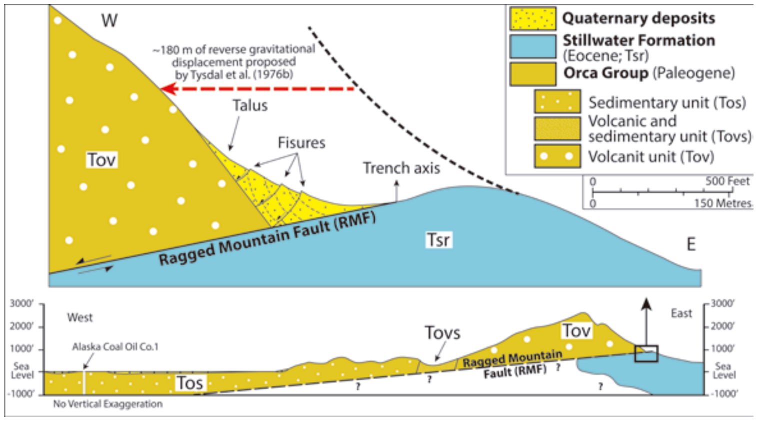

Fig. 3. Cross-sections of the RMF redrawn from Tysdal et al.(1976b), who postulated the Ragged Mountain is a west-moving detachment fault (or a planar block slide of 120 km^2), with the gliding surface controlled by a low-angle thrust. Bottom section shows overall structure; black box indicates area of enlarged section above. Enlarged section shows features at the range front and how the 180 m of normal fault slip was inferred.

Resolving the kinematics and Holocene rupture history of the RMF was a significant goal in the Saint Elias Erosion and Tectonics Project (STEEP), a major interdisciplinary study of the Saint Elias orogen that was supported by the Continental Dynamics Program of the National Science Foundation. Although the RMF is defined as a Quaternary-active fault (Koehler, 2013), the controversy about its late Quaternary slip sense and rate must be assessed via three aspects.

Aspect #1: is the normal slip sense inferred from Holocene scarps and troughs by Tysdale et al. (1976b) correct? We know that even historic thrust-fault surface ruptures have been accompanied by secondary extensional fault scarps (e.g., the M7.1 El Asnam, Algeria earthquake of 1980; Philip and Meghraoui, 1983), so the antislope scarps may be secondary coseismic features that do not reflect the slip sense of the master fault.

Aspect #2: if the scarps represent postglacial normal slip on the master RMF, is that slip passive gravitational sliding (decoupled from the crust) or active tectonic faulting that extends through the crust?

Aspect #3: if the normal slip is tectonic, how can crustal extension at a rate of ~18 mm/yrbe reconciled with the transpressional plate tectonic setting of the RMF? These were the questions that drove our investigation.

The investigation site is also an excellent natural laboratory for gaining insight into the poorly explored tectonic landscapes associated with active thrusts accompanied by secondary bending-moment and flexural-slip faults, as well as the kinematics of the different structures (e.g., Philip and Meghraoui, 1983; Audemard, 1999; Eusden et al., 2005; Kelsey et al.,2008; Bruhn et al., 2012). Previously-published papers from STEEP (Li et al., 2010;McCalpin et al.,

2011) describe Holocene gravitational deformation (sackung) slightly farther east in the Yakutat Terrane, where rapidly rising mountains composed of weak rocks are falling apart due to gravitational failures.

2. Materials and Methods

In summer 2005 our team spent one week of reconnaissance on the central third of the RMF, followed by 1.5 weeks mapping, measuring, and trenching scarps in summer 2006. Fault traces were initially mapped on aerial photographs, but by 2006 lidar DEMs were available and we transferred mapping to them. Scarp profiles were measured in the field with a laser rangefinder (Advantage Laser Products) that provided azimuth, inclination, and horizontal and vertical distance values. The profiles were then checked later against DEM-generated cross-sections. Five trenches were dug by hand, of which three yielded well-expressed stratigraphy and structure, and datable deposits.

2.1 Luminescence (OSL) sample processing and age analysis

Luminescence samples were processed by the Utah State University (USU) Luminescence Laboratory in Logan, Utah. Sample processing followed standard procedures involving sieving, gravity separation and acid treatments with HCl and HF to isolate the quartz component of a narrow grain-size range, usually 90-150 μm. The purity of the samples was checked by measurement with infra-red stimulation to detect the presence of feldspar. Sample processing procedures followed those outlined in Aitken (1998) and described in Rittenour et al. (2003, 2005). The Lab followed the single-aliquot regenerative-dose (SAR) procedures for dating quartz sand (Murray and Wintle, 2000, 2003; Wintle and Murray, 2006). The SAR protocol includes tests for sensitivity correction and brackets the equivalent dose (De) the sample received during burial by irradiating the sample at five different doses (below, at, and above the De, plus a zero dose and a repeated dose to check for recuperation of the signal and sensitivity correction). The resultant data were fit with a saturating exponential curve from which the De was determined. The reported De was based on the mean and standard deviation from the measurement of at least 20 aliquots of sand mounted on a 2-mm diameter area of the measurement disks. Dose-rate measurements were determined by chemical analysis of the U, Th, K and Rb content using ICP-MS and ICP-AES techniques. The contribution of cosmic radiation to the dose rate was calculated using sample depth, elevation, and latitude/longitude following Prescott and Hutton (1994). Dose rates were calculated based on water content, sediment chemistry, and cosmic contribution (Aitken, 1998).

3.The Ragged Mountain Fault

Our helicopter reconnaissance covered the entire RMF, but detailed field studies were restricted to a ~ 5 km-long section of the fault near the center of its broad arc.In this section surface faulting is best expressed by four types of landforms, from west to east: (1) long, linear antislope scarps on the lower part of the range front escarpment; (2) a trough at the toe of the escarpment (termed a “trench” by Tysdal et al., 1976b); (3) discontinuous, sinuous thrust scarps at the escarpment toe; and (4) swarms of closely-spaced, parallel ridges and troughs on a gently east-sloping footwall bench, underlain by the steeply-dipping Stillwater Formation.

3.1 Bedrock Stratigraphy and Structure

The RMF was traditionally interpreted as a low-angle, east-verging thrust fault that placed Paleocene rocks over Eocene rocks. The Paleogene accretionary complex here is represented by the late Paleocene-early Eocene Orca Group, a series of metamorphosed sedimentary and volcanic rocks intruded by late early Eocene granitic (Tysdal et al., 1976a, b; Winkler and Plafker, 1993). The Orca Group, with steep westward dip in Ragged Mountain, comprises three units in ascending order. Volcanic unit Tov (Fig. 3) is dominated by resistant pyroclastic rocks and basalt flows and underlies the range crest and eastern escarpment. A volcanic and sedimentary unit (sandstone and volcanics; Tovs in Fig. 3) and a sedimentary unit (flysch sequence; Tos in Fig. 3) crop out on the western flank of the range. The footwall of the RMF is composed of the Eocene Stillwater Formation (Tsr in Fig. 3), locally intruded by spatially restricted mafic intrusive rocks (Tysdal et al., 1976a, b; Winkler and Plafker, 1993). The Stillwater Fm. is composed of black thin- to medium-bedded carbonaceous micaceous siltstone and sandstone deposited in deep marine environments. On the RMF footwall the formation is tightly folded and beds have been differentially eroded (harder sandstone vs. softer siltstone and coal), giving the terrain a striped appearance.

The geometry of the RMF at depth is poorly constrained. Tysdal et al. (1976a, b) and Winkler and Plafker (1993) interpret a planar low-angle (8°W) thrust that truncates steeply dipping rocks on both walls (i.e., footwall and hanging-wall ramp). Recently, Heinlein et al. (in press) postulated that the RMF is a relatively steep thrust (>30°) with a ramp near the surface. This interpretation is based on geomorphic mapping of uphill-facing normal fault scarps along the east flank of Ragged Mountain and numerical modeling that couples thrust slip over a ramp and extension in the hanging-wall. Surface mapping shows that strike of the strata on both sides of the RMF tends to be parallel to the trace of the fault, veering from NNW in the northern sector to

NNE in the southern zone. The westward dips in the upper plate (Orca Group) range from 75° to 25°. In the footwall, the Stillwater Formation shows subvertical to steep dips, typically above 70°.

3.2 Geomorphology and Quaternary Stratigraphy

The RMF can be subdivided into four linear sections of differing strike (Fig. 4). The North Section is at least 14 km long and strikes N25°W. The Central Section is 10 km long and strikes roughly north. We subdivide it into a North Central subsection 5 km long striking N5°W, and a South Central subsection 5 km long striking N7°E. The South Section is at least 8 km long and projects offshore; it strikes N26°E. Compared to the convergence vector of the Yakutat and North American plates (oriented N31°W), the convergence angles of these four sections range from only 6° (at the north) to 57° (at the south). Accordingly, the geomorphic expression of the RMF varies among these sections. The North Section has the most linear range front-piedmont slope break and is dominated by a very long linear antislope scarp that parallels the range front but lies 50-100 m above the slope break. The low convergence angle of this section suggests it would accommodate nearly pure strike-slip motion. The North Central sub-section contains the same linear antislope scarps on the range front, but in addition has a wide, shallow, 5 km-long topographic trough at the toe of the range front. This trough is as much as 180 m wide and was interpreted by Tysdal et al. (1976b) as the result of 180 m of normal-fault backsliding of the hanging wall of the RMF during the Holocene. The convergence angle of this subsection (26°) is much larger than on the North Section. We first observed isolated, postglacial mountain-facing scarps on the footwall in this sub-section, which were later found (via trenching in the South-

Central sub-section) to represent young flexural-slip scarps in the overturned strata (Stillwater Fm.) of the footwall syncline.

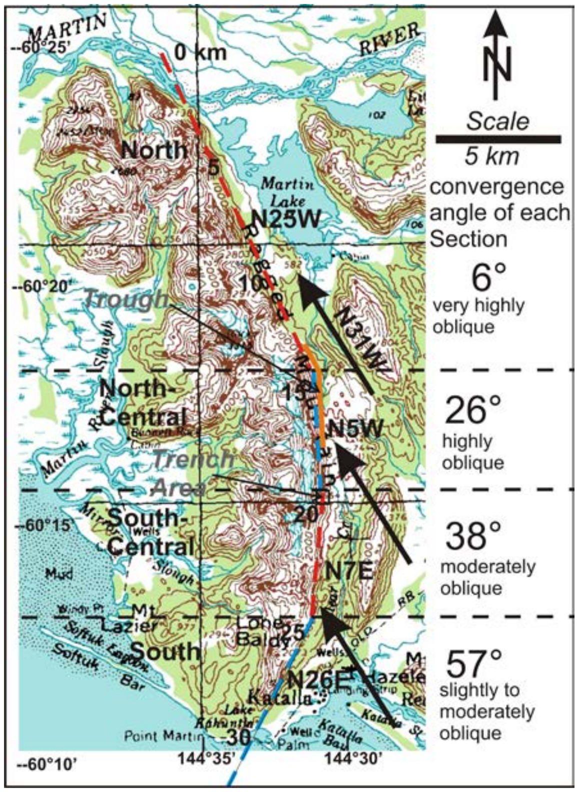

Fig. 4. The RMF (thick colored dashed lines) can be separated into four geometric sections (separated by dashed horizontal lines)based on strike. Convergence angles between each section and the Yakutat-North American plate convergence vector (N31°W) range from 6° in the north to 57° in the south (cf. Freymueller et al., 2008; Elliott et al., 2013). The trough of Tysdal et al. (1976b) and our Trench Area lie in the Central Section.

In the South Central sub-section the trough is absent and the long antislope scarp becomes discontinuous and then disappears. At the range-front slope break we find the first appearance of sinuous fault scarps with an asymmetric, convex scarp face (steepest at the toe), typical of thrust fault surface ruptures. On the footwall bench young flexural-slip scarps become longer and more numerous. These landforms suggest an increased component of convergence across the RMF, as does the larger convergence angle (38°). Our trench study area was situated in the northern part of this sub-section, using the well-preserved fault scarps as trenching targets. We did not make any field traverses on the South Section, but lidar shaded relief images show very few antislope scarps on the range front.

3.2.1 The Trough

The 5 km-long trough at the toe of the range front described by Tysdal et al. (1976b) is underlain by nearly vertical strata of the Stillwater Formation, as is the topographic bench east of the trough (Fig. 5a). The larger streams from the range front have cut across the trough and now exit through eroded gaps in its eastern boundary ridge (Fig. 5b). These streams have created several low terrace levels during incision. The trough floor flanking the streams contains a matching microtopography with two or three terrace levels which grade to those of the range-front streams. In the relatively un-incised part of the trough, the highest terrace within the trough (~2 m above stream level) marks the peak level of aggradation. This aggradation surface has subsequently been incised and now forms local drainage divides within the trough. An even higher, discontinuously-preserved terrace caps the eastern boundary ridge of the trough. There is no evidence of faulting or tilting of these surfaces. The set of geomorphic surfaces appears to reflect a simple history of episodic downcutting within the trough, probably starting at the end of the latest glaciation.

Fig. 5. Photographs of the trough. (a, left) The eastern margin of the trough (scarp to right of person) is formed by a near-vertical bedding plane fault in dark gray siltstone (Stillwater Formation). (b, right) View north down the axis of the trough, from north of the footwall drainage divide. Blue lines indicate drainages; yellow dashed lines, edges of valleys eroded through the trough margin; yellow dotted lines, highest alluvial terraces; red dotted line, local drainage divide within trough.

A small part of the trough exists in the south part of the North-Central section (Fig. 4), where incision into trough sediments by the headwaters of Clear Creek has been greater, up to 6 m. Incision created three geomorphic surfaces above modern stream level (Fig. 6). The highest surface (6 m above stream level) forms ridge-like remnants covered by roughly 1 m of loess. A more extensive terrace surface lies ca. 4.6 m above stream level, and is capped by thinner (~0.5 m) loess. The alluvium underlying this terrace is itself underlain by a bouldery diamicton that could be either till or debris-flow deposits. Inset within the 4.6 m terrace is a smaller 1.7 m terrace which has no loess cover. Streamcuts along the modern channel contain low (0.5-1 m) exposures of steeply-dipping to overturned black siltstones of the Stillwater Formation.

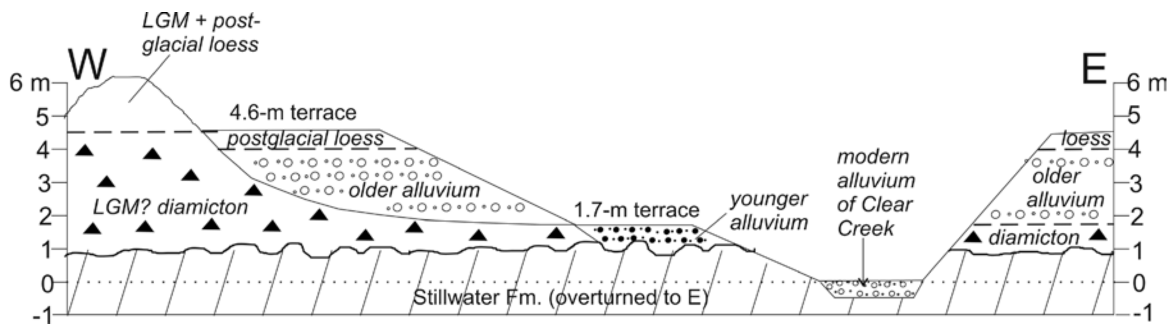

Fig. 6. Schematic cross-section showing morpho-stratigraphic units within the trough, south part of the North-Central section.

Lidar shaded reliefs reveal that the trough has a sinuous plan shape more like a fluvial channel, than like a tectonic landform bounded by planar faults (Fig. 7). The trough occupies a lowland bounded by range-front scree cones (on the west) and diamicton deposits (on the east), which form a discontinuous cover over the footwall bench underlain by the subvertical Stillwater Formation. If the diamicton represents LGM till, it is possible that the trough was formed by ice-marginal drainage along the edge of the LGM ice sheet. The trough parallels bedding planes of weak siltstones of the Stillwater Formation, so the trough could also be an erosional strike valley. Such an origin is compatible with the multiple terraces within the trough.

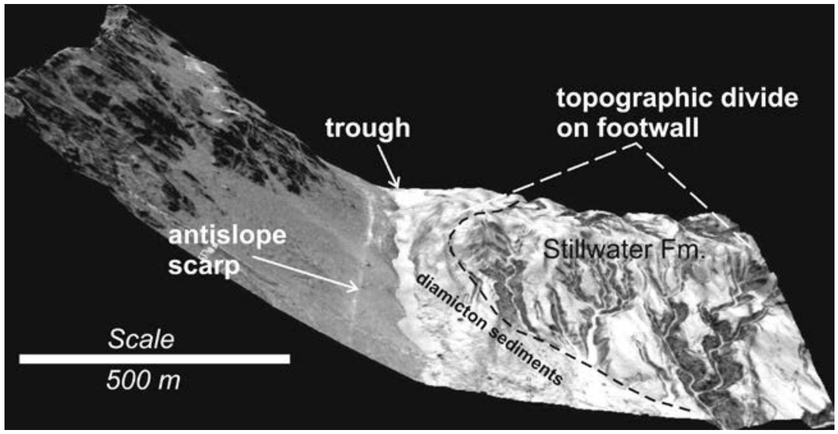

Fig. 7. Lidar slopeshade of the trough at the footwall divide, looking north. Highest point in trough is 435 m a.s.l.

3.2.2 Antislope Scarps

The most prominent tectonic landforms on the northern half of the RMF areantislope (uphill-facing) scarps that range-front cross scree surfaces. Antislope scarps dominate the North Section, but also exist in the Central Section. These uphill-facing scarps traverse the range front escarpment, parallel to contours but roughly 50-100 m above the toe (Fig. 7). Scarps range from 0-2.5 m high (with a vertical separation of 0-8 m, depending on slope gradient). The antislope scarps vary in their transverse profiles, from scarp faces steeper than the angle of repose (usually cored by shallow bedrock), to angle-of-repose scarp faces developed in colluvium, then to subdued scarp faces, and finally to subhorizontal benches with no scarp face. Regardless of profile shape, the apparent vertical separation can be measured by projecting the upthrown geomorphic surface over the downthrown surface. If these two surfaces are the same age, then the apparent vertical separation is also the true net vertical separation since deposition of the geomorphic surface.

Fig. 8 shows how vertical separation across the antislope increases with increasing age of the faulted alluvial-colluvial surfaces. Very young alluvial fans and talus cones bury the scarp, indicating no detectable displacement since their deposition. On young (late Holocene?) alluvial fans vertical separation of the faulted surfaces is about 2.5 m. On intermediate and old fans (early to mid Holocene?), vertical separation is 4.2-5.1 m. The oldest landform in the area (“old slide”; purple on Fig. 8) is much more incised than the other surfaces and is cut by an eroded, valley-facing scarp 10 m high (magenta line with hachures within purple polygon on Fig. 8) that appears to be separated from the sharp antislope scarp by a graben. The old slide deposit may be late Pleistocene and shows vertical separations across the antislope scarp of 7.8-8.2 m. If we assume that the smallest vertical separation (2.5 m) resulted from a single displacement event in the late Holocene, then the larger vertical separations may represent two displacement events since early Holocene, and three events since the late Pleistocene. Alternatively, single-event separations may be smaller than 2.5 m (see Trenching section, Trench 1), which would equate to more events.

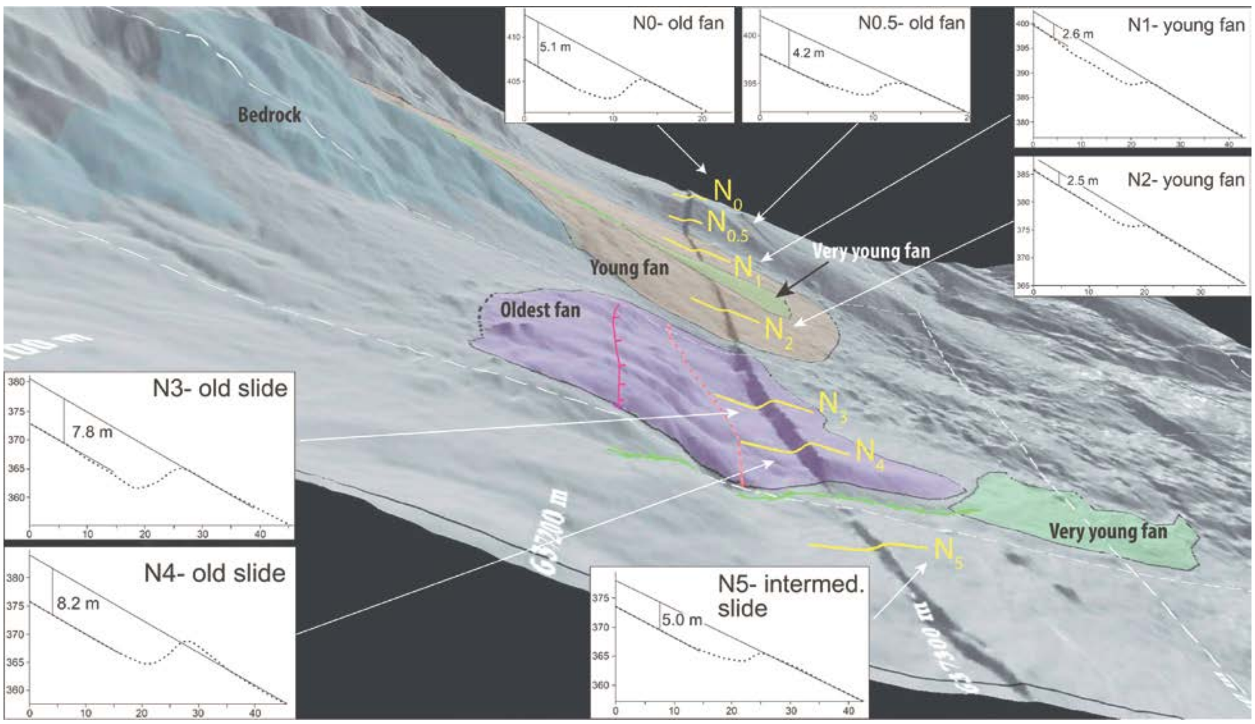

Fig. 8. Oblique lidar hillshade of the antislope scarp (dark band at center) looking north along strike. The height and width of the scarp face can be seen to increase on deposits of increasing age (green [no scarp]-orange-unshaded-purple [largest scarp]).

Another way to distinguish the age of displacements on antislope scarps is to observe how they interact with thin talus and rockfall deposits of different ages. At some antislope scarps talus transport is stopped by the scarp, so the scarp is older than talus (Figs. 9a, b, f). On other scarps talus appears to continue across the scarp with a uniform thickness, in which case the scarp is younger than talus (Figs. 9c, Supp. Fig. 2). At some scarps younger talus is stopped by the scarp but older talus is found downslope of scarp, so the scarp developed after the old talus but before the young talus (Fig. 9e). On talus that has been faulted, slabby blocks have been rotated up to lie parallel to the scarp face, similar to the “shear fabric” observed in faulted gravels in paleoseismic trenches. Such a dip is an unlikely primary orientation for a clast that had rolled up against a scarp. The highest scarp faces exceed the angle of repose and expose bedrock in the scarp face (Figs. 9g, h). Based on the above observations, there have been at least two displacement events of (Holocene) talus on the antislope scarp.

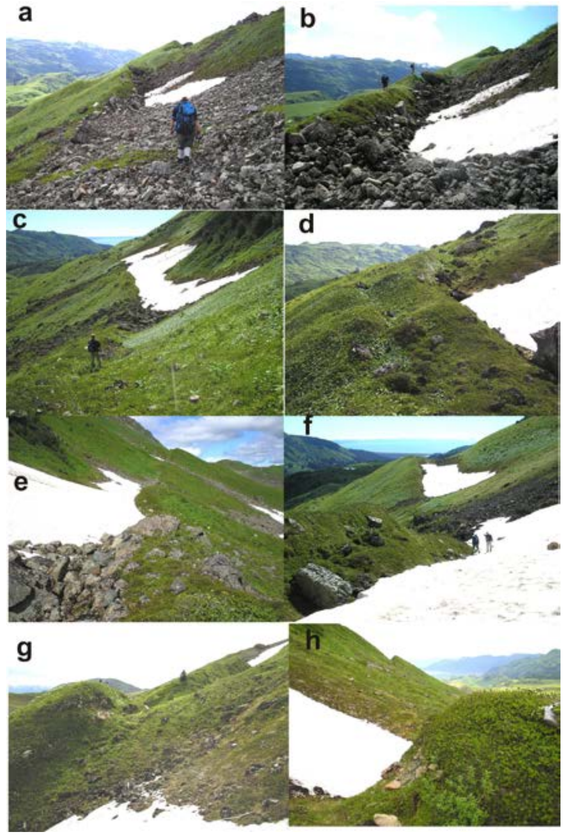

Fig. 9. Profile views of steep antislope scarps in the southernmost part of the North Central subsection (between 60.262°N and 60.267°N). All views are to the south except for “e” and “h”.

According to Fig. 4, the long, linear antislope scarp in the North Section should preserve the best evidence for lateral offset, given its low convergence angle. Unfortunately, the talus slopes crossed by this scarp contain very few linear landforms (piercing lines) with which to identify and measure lateral offsets. We were able to see only two probable lateral offsets, one at the northern end of the North Section at the limit of lidar coverage (UTM northing 6693600m), and another 4.5 km farther south near the middle of the North Section (UTM northing 6688900m; see Electronic Supplement). At both of these locations the lateral misalignment of the true right (southern) edges of alluvial fans was right-lateral (RL). The vertical separation across the best-developed antislope scarps (on the oldest surfaces) at these two sites is a consistent 3.5-3.7 m, whereas the apparent RL separation is a consistent 10-12 m. However, as described in the

Discussion, the apparent RL separation may in fact result from uplift of a ridge-like landform on the downslope side, rather than a true tectonic lateral offset.

3.2.3 Thrust Scarps

A discontinuous, sinuous, valley-facing scarp liesat the toe of the range front, with the steepest part of the scarp profile at the bottom. This profile geometry has been associated with thrust fault scarps (e.g. McCalpin and Carver, 2009, p. 329), created as the basal fault plane thrusts forward at a low angle and the entire scarp advances over and buries previous scarp-derived colluvial deposits. The oversteepened scarp also exhibit springs and oil seeps at its base, which are not observed at other scarps. The thrust scarp is most continuous in the northern part of the South-Central subsection, in a 1 km-long reach between 6682500 m N and 6683500 m N on the UTM grid (Fig. 10).

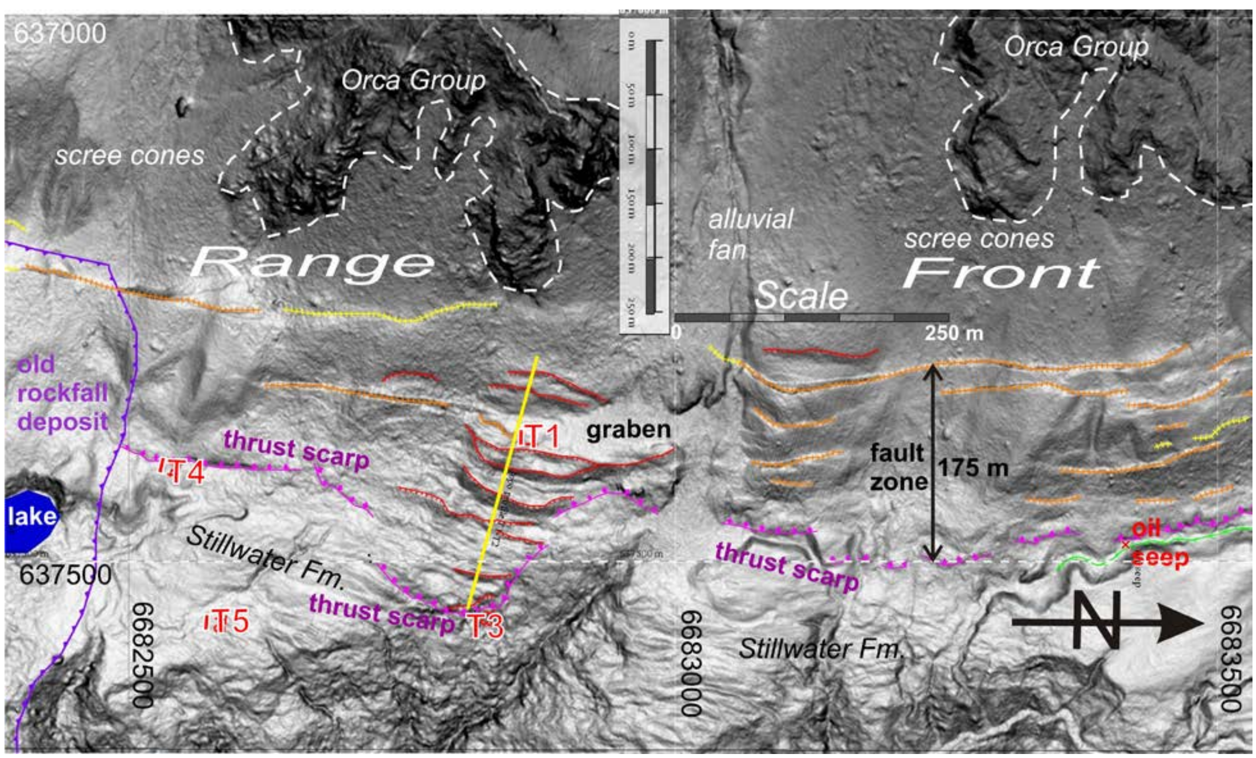

Fig. 10. Lidar slopeshade of our trench study area (location shown on Fig. 4). Orange hatched lines, uphill-facing scarps and troughs, well-developed; yellow hatched lines, discontinuous uphill-facing scarps; red lines, downhill-facing scarps; purple lines, thrust scarp, diamonds on upthrown side. Trenches and oil seep from thrust fault labeled in red. Thick yellow line shows topographic profile line (Fig. 11b).

Near the center of the trench study area the oversteepened thrust scarp swings east about 100 m onto the footwall, forming an arcuate lobe about 150 m wide along strike (Fig. 11). Within this lobe are an anomalous number of uphill-facing scarps which do not extend beyond the lobe margins. Additionally, there are at least eight low, mountain-facing scarps on the footwall bench directly east and south of the lobe. This concentration of tectonic landforms of different types in a small area dictated that our detailed study area should be here.

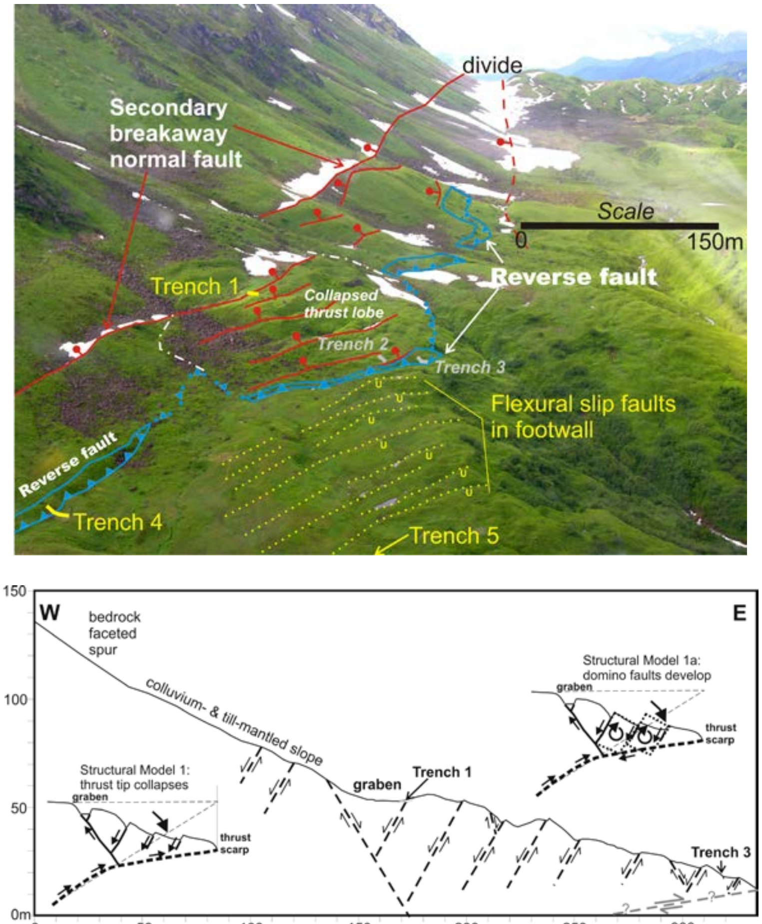

Fig. 11. Top, oblique helicopter view of the RMF looking northward from the collapsed thrust lobe (center) toward the drainage divide on the footwall. Blue lines, thrust scarps; red lines, normal fault scarps; yellow dotted lines, near-vertical flexural slip faults of the footwall syncline. Bottom, topographic profile from the range front through the collapsed thrust lobe. Thrust fault daylights in bottom right corner. The right two-thirds of this line of section is shown as a solid yellow line in Fig. 10. Subsurface contacts are inferred..

Where the lobe joins the range-piedmont slope break, we observed the largest graben seen anywhere along the RMF (185 m long by 35-55 m wide; labeled ‘graben’ in Fig. 10). This wide graben and the five large uphill-facing scarps downslope suggest that the entire lobe has been subjected to more east-west extension than any other site along the RMF. Our field interpretation was that the thrust tip had travelled so far onto the footwall here that it had collapsed and induced numerous secondary normal faults (Fig. 11b). We then sited our four trenches based on this conceptual model (see Trenching section).

3.2.4 Large Landslide Blocks in the South Section

The South Section of the RMF possesses the largest convergence angle of all the sections (57°) but lacks the typical tectonic landforms found in the other sections (long, linear antislope scarps on the range front; trough; small thrust scarps at the range-piedmont slope break). Instead, the South Section is dominated by large-scale block landsliding, something not observed in the other sections. The main slide block (outlined in yellow on Fig. 12) is 2.5 km wide, 0.6-0.7 km long, and 200-250 m thick, involving the entire range front. At its south end the block protrudes about 200 m eastward relative to the range front to the north and south, giving a rough estimate of eastward sliding. The head of the block is marked by a linear, east-facing headscarp (red in Fig. 12) as much as 75 m high. From the northwest corner of the slide block the headscarp continues north an additional 0.5 km. It first displaces a sharp (25 m high, 90 m wide) lateral moraine (LGM?) by 30 m down-to-the-east, indicating postglacial movement of the block. The scarp then continues north to form a ridge-top depression filled with lakes, similar to a classic sackung landform (a “doppelgrat”) formed by deep-seated gravitational deformation.

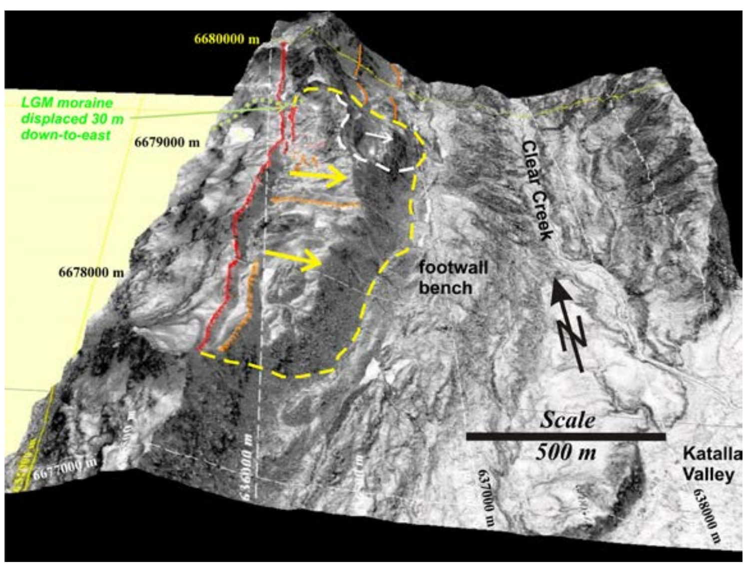

Fig. 12. Oblique lidar slopeshade of the RMF in a 3 km-long part of the South Section between about 6677000 m N and 6680000 m N, UTM coordinates. The slide block outlined in yellow has dropped down 50-75 m at the headscarp (red) and protruded out ~200 m onto the footwall bench.The northeastern corner of the slide block has failed in a secondary slump block (white outline) 460 m long, 310 m wide,

and ~190 m thick. The top of the block has slid down 150 m from its original position and back-rotated 25° down toward the curved headscarp.

4. TRENCHES

Within the trench study area we excavated five trenches by hand, all oriented east-west and crossing north-south scarps. Trenches 1, 4, and 5 yielded the best information (Figs. 10, 11). Trench 1 was excavated in a large graben upslope of the leading edge of the range-front thrust fault, at an elevation of ca. 325 m. Trench 4 was excavated across a thrust scarp 330 m south of T1, at an elevation of 285 m. Trench 5 was excavated 140 m east-northeast of T4 at an elevation of 273 m, across one of the many parallel, low, mountain-facing scarps that cut the 250 m-wide footwall bench.

4.1 Trench 1

Trench 1 crossed the eastern margin scarp of the large graben (Fig. 13) upslope of the collapsed thrust lobe, and exposed six fault zones, all but one of which are west-dipping normal faults (Fig. 14). Faults F1 through F3 underlie the 0.75 m-high west-facing scarp that bounds the east side of the graben. Fault F6 underlies a smaller (0.37 m-high) west-facing scarp within the graben. Faults F4 and F5 have no surface expression.

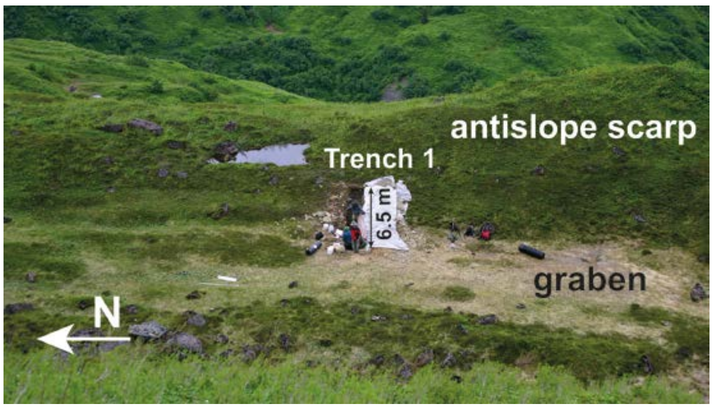

Fig. 13. Photograph of Trench 1 on the eastern margin fault of the large graben, looking east from the toe of the steep range front. White material to right of trench is the plastic rain cover. Three people are standing in the trench.

The six numbered faults have a minimum down-to-the-west throw of 1.8 m. The displacements of each fault on basal unit contacts are shown on Fig. 14 (lower right corner of log). The displacement pattern indicates that faults farthest from the graben axis experienced the oldest displacement. For example, displacement on fault F1 (earthquake 1) and later displacement on

Faults F2 and F3 (earthquake 2) offset late Pleistocene alluvial fan deposits, and predate 21.6±2.4 ka (OSL ages from Table 1). The third earthquake (earthquake 3) reactivated fault F2 (but not F3) sometime after 21.6±2.4 ka and 18.1±3.4 ka. The free face created during this event was composed only of coarse late Pleistocene alluvial fan deposits, which then eroded and formed the only colluvial wedge in the trench (unit 3).

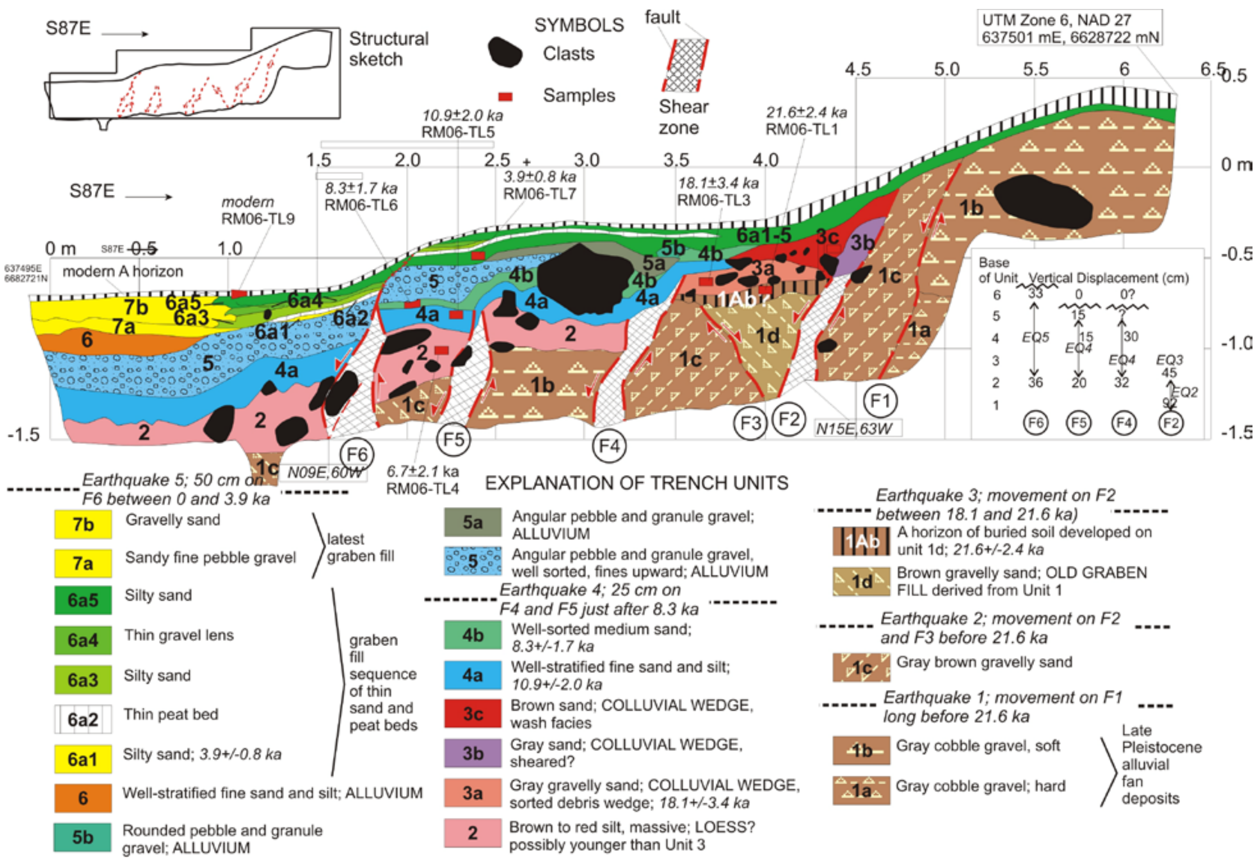

Fig. 14. Log of the north wall of Trench 1.

Table 1. Luminescence ages from Trench 1.

Ragged Mountain OSL Dates			All data from the Utah State University Luminescence Lab, Logan, Utah						
TRENCH	Lab No.	**Sample No.**	Unit	Depth (m)	No. of Disks	Dose Rate (Gy/ka)	De (Gy)	**Age (ka)**	Remarks
T1	USU-049	**RM06-TL1**	1Ab	0.37	21 (50)	0.76±0.05	16.47±6.23	**21.6±2.4**	close maximum age on earthquake 3 on faults F2-F3
	USU-051	**RM06-TL3**	3a	0.31	24 (40)	0.70±0.05	12.66±10.46	**18.1±3.4**	Minimum age on earthquake 3 on faults F2-F3
	USU-052	**RM06-TL4**	2			*suspended*		***6.7±2.1***	*predates earthquake 4 on faults F4 and F5*
	USU-053	**RM06-TL5**	4	0.42	22 (39)	0.71±0.05	7.77±5.97	**10.9±2.0**	predates earthquake 4 on faults F4 and F5
	USU-054	**RM06-TL6**	4	0.3	23 (39)	0.64±0.07	5.37±4.43	**8.3±1.7**	Closely predates earthquake 4 on faults F4 and F5
	USU-055	**RM06-TL7**	6a1	0.12	20 (33)	0.88±0.07	3.45±2.90	**3.9±0.8**	predates earthquake 5 on fault F6
	USU-057	**RM06-TL9**	7bA	0.05				**modern**	post-dates earthquake 5 on fault F6

The other hanging-wall strata in the trench younger than earthquake 3 are either well-sorted alluvial deposits from an axial stream (units 4, 5, and 7), massive silts (loess or sag pond sediments, unit 2), or thinly alternating sag pond peats and sands (unit 6). These units lap up against the toe of the colluvial wedge from earthquake 3, indicating that they were all deposited in the current large graben depression. Faults F4 and F5 deform the lower units in this section (2 and 4) but not the upper units (5 and 6), indicating younger movement than expressed on faults F1-F3. The youngest evidence for movement is on fault F6, which displaces all the units in the trench except unit 7, and forms a scarp on the present ground surface. All strata offset by fault F6 are displaced the same amount (33-36 cm), indicating that it formed in a single displacement event with no prior history.

The overall progression is younger faulting toward the graben axis, and abandonment of the more distal faults. Of the five earthquakes we can interpret, the earlier two are poorly dated (both considerably older than 21.6 ka), and the later three occurred roughly between 18.1-21.6 ka (earthquake 3), just after 8.3 ka (earthquake 4), and considerably younger than 3.9 ka (earthquake 5) but older than the 1964 M9.4 Anchorage earthquake, which did not cause rupture on the RMF(Tuthill and Laird, 1966). These ages suggest recurrence intervals of 9.8-13.3 kyr (EQ3 to EQ4) and 4.4-8(?) kyr (EQ4 to EQ5).

4.2 Trench 4

Trench 4 was excavated across an asymmetric scarp roughly 3-4 m high (Fig. 15). Rockfall deposits that cross the scarp appear to drape over the scarp face, and occasionally larger-than-average blocks are perched in a mid-scarp position. It is unlikely that the larger rocks, having more momentum than smaller rocks, would naturally come to rest on a steep scarp face, while smaller rocks kept going and were deposited below the scarp. A more likely interpretation of the large blocks is that they were deposited before the scarp formed, and were later uplifted and tilted on the scarp face.

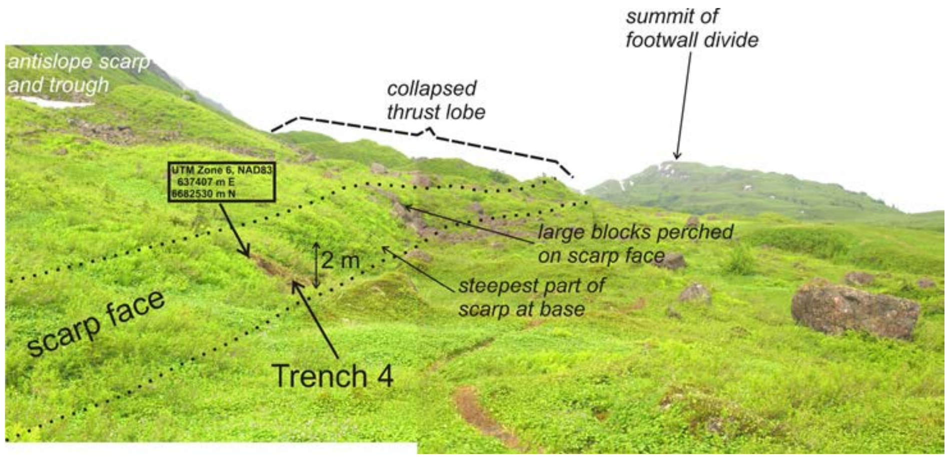

Fig. 15. Telephoto view of the thrust scarp (between dotted lines) and Trench 4. View to north toward the collapsed thrust lobe.

Trench 4 exposes only two fault zones, both west-dipping thrust faults (Fig. 16). Fault F1 dips 30°-40°W and displaces the unit 1b/1a contact a total of 64 cm (net slip in the plane of the trench wall), but has only displaced the top of 1b by 26 cm (in the most recent event, or MRE). Fault F2 dips 19°W and has displaced unit 2Bb 46-48 cm in its MRE (net slip; 28 cm throw), but its total displacement on the top of unit 1b is at least 105 cm (net slip). These differential displacements indicate multiple displacement events on each fault. All displacement events apparently postdate the sequence of alluvial strata on the footwall (unit 2), since it is abruptly truncated by fault F2 but is missing from the hanging wall, evidently eroded off the hanging wall (HW) prior to deposition of unit 4. Thrust displacement has rotated the once-horizontal alluvial deposits 25° valleyward on the hanging wall of F2 and 55° above F1.

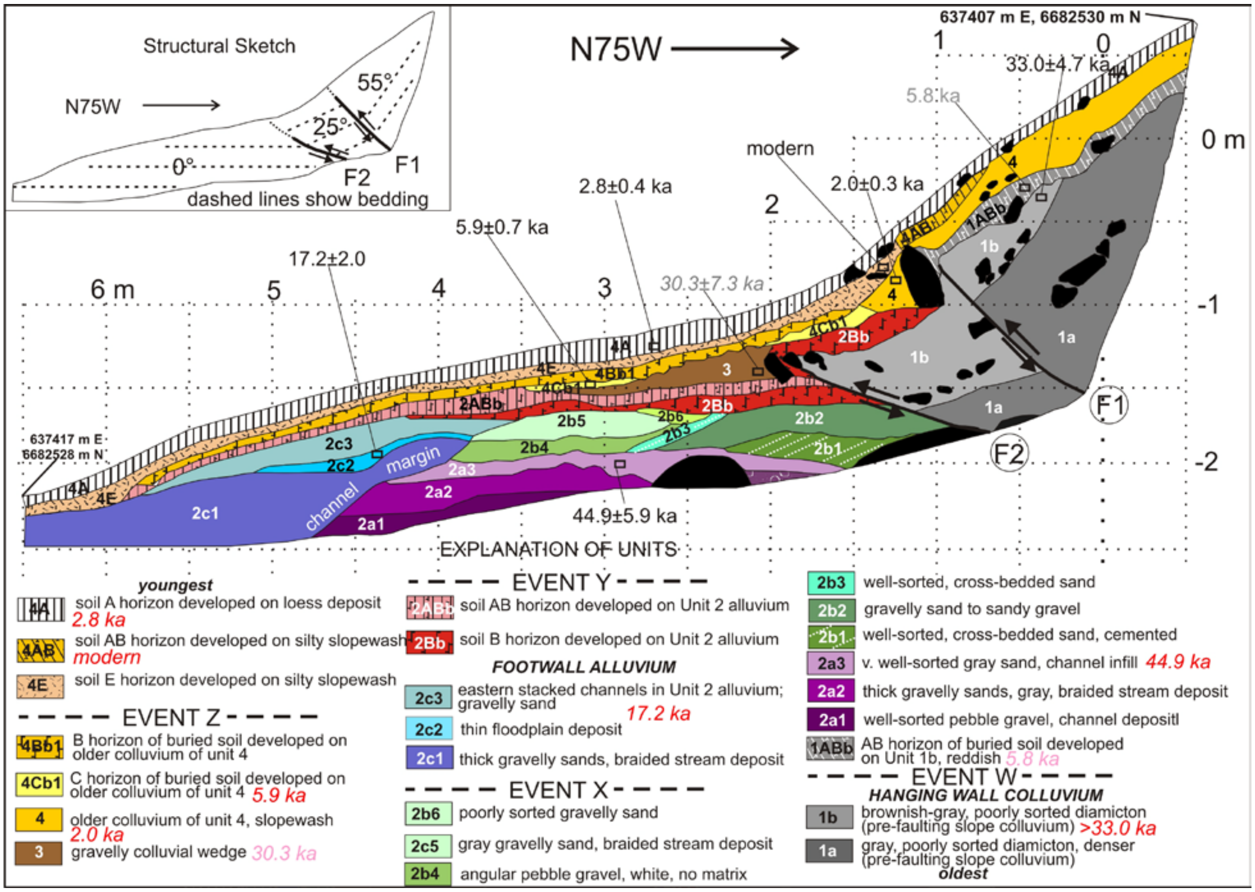

Fig. 16. Log of the south wall of Trench T4. OSL ages in black are final ages (mean and 2 sigma); those in gray are preliminary based on a small number of aliquots.

There is only one obvious colluvial wedge on the trench wall (unit 3, up to 20 cm thick), shed from the latest free face of fault F2. This displacement event must postdate unit 2ABb (unit 2Bb is offset 26 cm by F2) and predate the deposition of the colluvial wedge. The earlier displacement event(s) (amounting to ~70 cm of net slip) are not are not represented by a similar preserved wedge, suggesting that wedge(s) formed but were then removed by erosion (see retrodeformation sequence, Fig. S5).

Luminescence ages (Table 2) indicate that the multiple faulting events span a long time range, from prior to deposition of unit 2a2 (44.9 ka) until after the deposition of the lower half of unit 4 (2-3 ka). There are some age reversals and ambiguities with the older ages. For example, during logging we correlated alluvial units 2a2 and 2c2 based on lithology and thickness; they were separated by an east-dipping contact tentatively interpreted as a backthrust. However, OSL ages show the two units are very different in age, 17.2 ka for 2c2 and 44.9 ka for 2a2. A more reasonable interpretation is that the contact is an erosional channel margin, with much younger strata on the east (2c units) inset into older alluvium to the west (2a units).

Table 2. Luminescence ages from Trench 4.

Ragged Mountain OSL Dates		All data from the Utah State University Luminescence Lab, Logan, Utah						
TRENCH	Lab No.	**Sample No.**	Unit	Depth (m)	No. of Disks	Dose Rate (Gy/ka)	De (Gy)	**Age (ka)**
T4	USU-058	**RM06-tTL1**	4E	0.16				**modern**
	USU-059	**RM06-tTL2**	4	0.32	21 (35)	1.81±0.13	3.60±1.83	**2.0±0.3**
	USU-060	**RM06-tTL3**	4	0.22	21 (23)	1.90±0.12	5.39±3.54	**2.8±0.4**
	USU-061	**RM06-tTL4**	3			*suspended*		***30.3±7.3***
	USU-063	**RM06-tTL6**	1ABb			*suspended*		***5.81***
	USU-064	**RM06-tTL7**	1b	0.5	20 (55)	0.77±0.04	25.41±14.54	**33.0±4.7**
	USU-065	**RM06-tTL8**	4Cb1	0.27	21 (23)	1.22±0.11	7.25±2.39	**5.9±0.7**
	USU-066	**RM06-tTL9**	2d	0.74	20 (38)	1.09±0.05	48.88±25.90	**44.9±5.9**
	USU-067	**RM06-tTL10**	2i	0.42	20 (45)	0.90±0.05	15.47±7.05	**17.2±2.0**

The three youngest displacements events are marked on Fig. 16, bracketed by ages of 2.8-5.9 ka (Event Z), 5.9-17.2 ka (Event Y), and 17.2-44.9 ka (Event X). At least one additional displacement event prior to 44.9 ka (Event W) is required on F1 to justify the different displacements of units 1a and 1b. This suggests a temporal progression of thrusting toward the footwall (in-sequence thrusting; [McClay, 1992]), except for Event Z. A retrodeformation analysis containing four displacement events reproduces the present trench geometry (Fig. S5), but due to fluvial erosion of the hanging wall prior to 45 ka, the number of early events interpreted is a minimum.

4.3 Trench 5

Trench 5 was rather arbitrarily located across one of the many low, mountain-facing scarps on the footwall bench (Fig. 17). Due to the gentle slope of the bench and the underlying clayey, impermeable bedrock, groundwater table was very shallow and every scarp was accompanied by a linear trough at its toe filled with a lake or a marsh. We chose the driest trough we could find but still encountered groundwater at a depth of about 0.75 m. Our goals were: (1) to test if these scarps were erosional or tectonic; (2) if tectonic, what was the dip and slip sense of the underlying fault; and (3) what was the relationship between the fault and bedding planes in the Stillwater Fm.

Fig. 17. Telephoto view to the east over the footwall bench, showing the density of antislope scarps (red arrows). The deeply incised valley of Clear Creek is in the middle ground. In the background is the unnamed ridge between Clear Creek and the Katalla Valley, riddled with sackungen.

Trench 5 was 4 m long and as much as 1 m deep, oriented roughly east-west, perpendicular to the scarp and adjacent trough. There were no faults visible on the trench wall. Instead, the sag pond sequence was bent sharply upward from a dip of 11°-13°E beneath the trough to a dip of 44°-73°W beneath the scarp face (Fig. 18). The asymmetric fold has a total vertical amplitude of 1.25 m, measured on the top of the oldest Quaternary deposit (unit 1, a diamicton that may be colluvium or clast-poor LGM till).

The sharp fold, developed on rather plastic deposits, should have placed material in the inner hinge zone under compression, and in fact there is a weak parasitic fold on the east limb in unit 2, but no discrete reverse fault. Given the moist, clay-rich nature of all units, they may have been too plastic to sustain discrete faulting within 1 m of the ground surface, and instead formed a fault-propagation fold. The tip of the presumptive fault lies somewhere beneath the trench floor, but due to high groundwater we were unable to expose it.

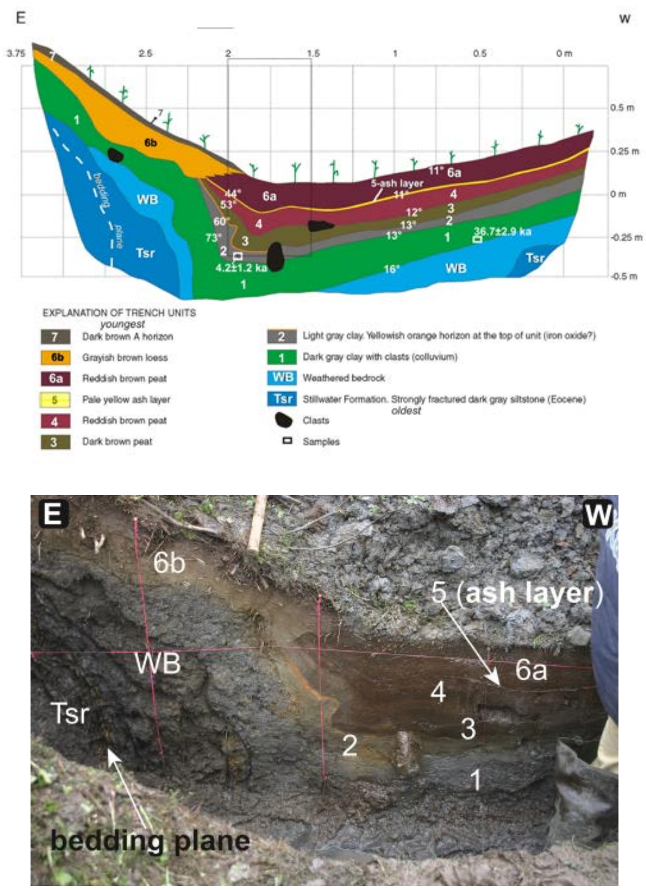

Fig. 18. Top, log of the southern wall of Trench 5. Blue and green units predate the formation of the scarp and trough, based on their uniform lithology and thickness along the trench wall. Gray, brown, and red units were deposited during and after the formation of the trough. White labels show unit numbers and dip of strata in degrees. Bottom, photo of south wall. Tsr, Stillwater Fm. WB, weathered bedrock. Gray stony clay deposits atop WB (1) are colluvium (or till) that predates the scarp. Brown strata 2-6 are sag pond sediments deposited after formation of the scarp.

We collected only two luminescence samples here (Table 3) because no discrete faults or event horizons were exposed in the trench. The two samples show that a long hiatus ensued between deposition of the youngest pre-trough deposit (unit 1, 36.7±2.9 ka) and that of the oldest trough deposit (unit 2, 4.2±1.2 ka). Unit 1 maintains a uniform thickness across the fold axis, suggesting it was deposited before the fold scarp formed. After the fold scarp formed, the upper half of unit 1 was eroded on the scarp face and replaced by loess (unit 6), while in the trough sag pond sediments began accumulating starting ~4.2 ka. This indicates the fold scarp formed just prior to 4.2 ka.

Table 3. Luminescence ages from Trench 5.

Ragged Mountain OSL Dates			All data from the Utah State University Luminescence Lab, Logan, Utah						
TRENCH	Lab No.	**Sample No.**	Unit	Depth (m)	No. of Disks	Dose Rate (Gy/ka)	De (Gy)	**Age (ka)**	Remarks

T5	USU-068	**RM06-fsTL1**	1	0.47	23 (31)	1.80±0.10	65.97±16.34	**36.7±2.9**	probable LGM till with some inherited luminescence
	USU-069	**RM06-fsTL2**	3	0.37	9 (15)	0.73±0.12	3.08±2.08	**4.2±1.2**	oldest unit post-scarp formation

Folding of the trough units has continued since 4.2 ka, as evidence by the progressive tilts of units 2 through 5 (synsedimentary deformation). Two lines of evidence suggest this is the result of creep deformation. First, dips on each fold limb increase down section, with no abrupt change (angular unconformities) at any stratigraphic level (i.e., no growth unconformity or cumulative wedge-out). Second, there are no scarp-derived colluvial deposits interfingered with the fine-grained sag pond silts and peats, which indicates there has never been a sudden and high enough surface rupture (free face) to break the tundra mat and expose fresh sediments. In this regard the deformation in Trench 5 is very different from that in trenches 1, 3, and 4, all of which show indicators of abrupt displacement events.

5. DISCUSSION

5.1 Style of Deformation

Based on our geomorphic mapping and trenching, we interpret the RMF as a reverse-oblique fault with an increasing component of lateral slip to the north, due to the variable orientation with respect to the plate convergence vector. In fault sections with the higher convergence angles we observed a complex suite of tectonic landforms (graben and collapsed thrust wedge with antislope scarps in the upthrown block, and swarms of flexural-slip scarps in the footwall). This same suite of landforms was observed after the well-documented historic thrust fault event at El-Asnam, Algeria (1980,M7.1; Philip and Meghraoui, 1983). The easiest tectonic ruptures to see at El Asnam (as at Ragged Mountain) were the secondary normal fault scarps created by collapse of the thrust tip (Fig. 19). In the earliest reconnaissance of the 1980 ruptures, Shah and Bertero (1980) observed "*In most places, the displacement on the secondary high angle normal faults produced scarps that are more pronounced than those along the primary thrust fault.*" We believe a similar situation exists on the RMF, and suspect that outside of our detailed study area there are many more undiscovered thrust scarps.

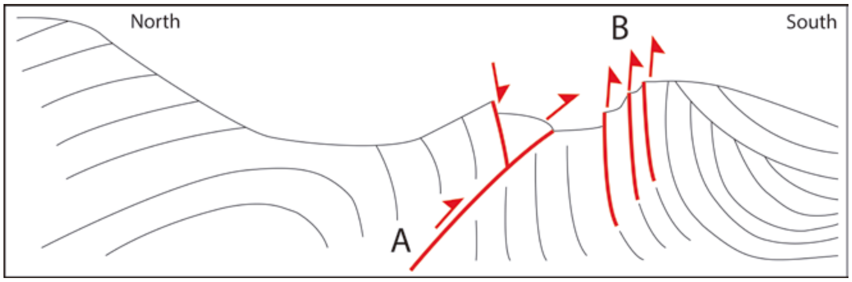

Fig. 19. Diagrammatic cross section of coseismic thrusting, normal faulting and flexural-slip faulting at Kef el Mes, 1980 El Asnam earthquake, Algeria; after Philip and Meghraoui (1983). The earthquake-generating reverse fault is at A. Note the collapsed thrust wedge controlled by a shallow normal fault. Coseismic flexural-slip faults at B were produced by renewed folding of the footwall syncline.

Our trenches across the primary thrust and secondary normal faults in the hanging wall display typical fault structures and fault-induced sedimentation seen in many paleoseismic trenches. In the Trench 1 graben the outboard normal faults developed first and then were abandoned when younger faults developed closer to the graben axis, mimicking the fault migration pattern observed at the crustal scale (e.g., Dart et al., 1995). The thrusts in Trench 4 obey all the usual relationships observed in many other thrust trenches (McCalpin and Carver, 2009); they project toward the toe of the scarp, the steepest part of the scarp profile; they override younger footwall strata and truncate them; and thrusting migrates through time toward the footwall. Of the three latest displacement events only the middle one has a well-preserved colluvial wedge, but the absence of older wedges can be explained by fluvial erosion at the scarp base, and by erosional stripping of wedges by uplift of the hanging wall and forward rotation of the hanging wall, and development of the oversteepened (42°) scarp face.

5. 2 Ambiguities Between Landforms and Kinematics

Three kinematic aspects of the RMF have some remaining ambiguity: (1) the exact kinematics of the long, linear antislope scarps; (2) why Trench 5 appears to exhibit creep deformation whereas all other structures display episodic displacement; and (3) why the South Section (the most convergent) spawned such large landslides and gravitational spreading features.

5.2.1 Antislope Scarps

Early in the STEEP project the structural geology team speculated that the antislope scarps might be sackungen, formed by deep-seated gravitation slope deformation (DSGSD). However, sackungen typically form high on mountain ridges, not at the toes of escarpments where there is no gravitational potential. In some ways the RMF antislope scarps resemble “ridge rents”, first described in New Zealand on strike-slip faults (Cotton, 1950). Linear, uphill-facing scarps have been now widely described in the literature, mostly on strike-slip faults (e.g. McCalpin, 1996; Schermer et al., 2004; Briggs and Wesnousky, 2005; Langridge and Berryman, 2005; Fraser et al., 2009; Van Dissen and Nicol, 2009; Clark et al., 2011; Barrell, 2013; Tibaldi et al., 2015; Li et al., 2017; Litchfield et al., 2018) but occasionally on the hanging walls of reverse-oblique faults (Eusden, 2005; Strom et al., 2015; Arrowsmith et al., 2016; Morell et al., 2017).

However, if the linear antislope scarps were formed by strike slip (or highly oblique) slip, shouldn't they laterally displace landforms along strike? We did not notice any such offsets in the field, but more recently reexamined the lidar DEM, especially in the North Section which has the smallest convergence angle. Over the 8 km length of the North Section we found only two poorly-defined lateral misalignments, both right–lateral (RL) (Figs. S3, S4). If the Ragged Mountain fault is really a suture between the Yakutat Block (to the east) and the North American plate (to the west), its indentation into the NA plate should be expressed as left-lateral slip. One possible explanation is that the apparent RL misalignment of relatively sharp slope breaks at the lateral margins of alluvial fans/cones (in both cases measured on the true right sides of fans) is a result of vertical displacement of the fan margin by the antislope scarp. Such uplift raises the entire fan landform on the downslope side of the fault, and this 'emergence' makes the fan wider on the downslope side of the fault. This widening should result in an apparent RL misalignment of the fan margin on the true right side of the fan and a matching LL misalignment on the true left side of the fan (Fig. S6). The magnitude of the misalignment is a function of the amount of vertical uplift and the slope of the fan margin parallel to the fault scarp. This geometric approach is a special case for the two fan margins that were sharp enough to consider a piercing line. The general case all possible fault/landform geometries is described by Mackenzie and Elliott (2017).

For the site at the northern end of the North Section (Fig. S3), where vertical separation is 3.7 m and the fan margin slope (labeled "riser") has a gradient of 12° parallel to the fault, a RL misalignment of 17.4 m is predicted (as opposed to the 10 m measured on the lidar DEM). The alluvial fan margin slope on the true left side does not have sharp enough slope break at its base to use as a piercing line, so a similar comparison cannot be made there. The critical issue here is that the two apparent RL misalignments of lateral fan margins could be explained by purely vertical movements, which would then moot the problem of having RL misalignments on a fault that, based on tectonics and seismology, should have LL slip.

5.2.2 Flexural-Slip Faults

Trenching investigations in different regions have documented episodic displacement on flexural sip faults of both tectonic and gravitational origin. For instance, Kelsey et al. (2008) infer that bedding-plane faults above an active wedge thrust in the Seattle fault zone, USA, represent independent seismic sources. Gutiérrez et al. (2014) found clear evidence of stick-slip displacement on flexural-slip faults related to the “unfolding” of the Grand Hogback Monocline, Southern Rocky Mountains, induced by deep-seated salt dissolution. How is it possible to have creep behavior in Trench 5 but episodic displacement in Trenches 1 and 4 only 100 m away? The answer may lie in the timing. The most recent displacement event (MRE) in Trenches 1 and 4 is dated as modern to 3.9 ka, and 2.9-5.8 ka, respectively. Thus it is possible that the sudden formation of the fold scarp just before 4.2 ka was contemporaneous with the MRE. In the ensuing 4.2 ka there have been no further displacement events at Trenches 1 and 4, yet the fold in Trench 5 appears to have continued slowly tightening up to present. This tightening could be interpreted as interseismic crustal deformation, or as a shallower delayed response of the footwall syncline (in ductile strata) to the rapid displacement of the stronger, brittle hanging wall rocks during the MRE.

5.2.3 Origin and Significance of Large Landslide Blocks and Sackungen

We expected the most convergent (South) section of the RMF to have the best-expressed thrust scarps. Instead, thrust scarps were undetectable, and the range front was dominated by gravitational extensional deformation (landslides and sackungen) that involved the east face (Fig. S7). How can we reconcile these contradictory kinematics? The most likely explanation is that higher convergence angles result in greater heightening and oversteepening of the range escarpment, creating favorable conditions for the development of gravitational slope deformations and landslides. It is likely that the dip of the master thrust beneath the range front becomes so shallow near the surface (hanging wall advancing over the footwall bench) that it has functioned as a potential sliding plane for “undermining” the steep range front.

A similar case of range-front reverse faults flattening to horizontal and then beyond, becoming failure planes for landslides, are described in southern California (Sierra Madre fault) by Crook et al. (1987). They call these landslides “thrust-rooted slides”, which “*consist of highly fractured* *masses of crystalline basement rock that have moved downhill on slide planes effectively continuous with the thrust planes above and behind them, so that the slide-thrust surface takes on an antiform configuration. The slide mass is derived directly from the upthrown block of the thrust, so that there is no clear dividing line between the part of the mass that should be termed a slide and the part that represents the upthrown block*." (Crook et al., 1987, p. 41). The size of these southern California landslides (~250 m long; Fig. S8) is, however, much smaller than the block slide on Ragged Mountain (700 m long).The "thrust-rooted slides" and the collapsed thrust wedges fit with the epiglyptic thrust concept of Mattahuer (1973), proposed for large subaerial landslides derived from the rejuvenating upthrown block of active thrusts (e.g., Atlas Mountains, Northern Africa). The trigger mechanism of these large failures is unknown. Seismic triggering is possible, but could have originated from M~7 earthquakes on the RMF, or from M8-9 earthquakes on the eastern Aleutian megathrust.

5.3 Implications of the Tectonic Geomorphology for Regional Tectonics

The RMF lies in a complex zone of deformation at the western edge of the Yakutat collision zone. GPS data and seismicity indicate complex ongoing strain patterns in the vicinity of the RMF. Geologic studies show a complex history of refolding of earlier folds about vertical axes during the latest deformation (Bruhn et al., 2004) and suggest the trace of the RMF reflected vertical axis folding of the suture (Pavlis et al., 2014). Thus, the kinematics of the RMF represents a critical element in the local manifestations of this ongoing deformation, and the controversies on the nature of the fault prior to this study led to major ambiguities on how strain was accommodated in this region.

The results of this study and a related study by Heinlein et al. (in press) indicate that the RMF is not a normal fault. The trough that parallels the fault in the central segment (Figures 2, 4, 6, 8),and used by Tysdale et al. (1976b) to infer large magnitude normal displacement, is not a fault related feature; rather this trough is an erosional feature generated, at least in part, during LGM glaciation. The extensional scarps that follow the fault trace are easily explained by hanging wall flexure above a thrust that is largely blind aside from the exposed scarps that were trenched in this study. Indeed, the theoretical analysis of Heinlein et al. (in press) suggests the extensional scarps are closely linked to fault geometry, with an inference that the main fault at depth is relatively steeply dipping, but ramps to low-dips near the surface. Geomorphic and trenching evidence suggest that the antislope, thrust, and flexural-slip faults have movedcontemporaneously, suggesting a structural connection.

Recognition that the RMF is indeed a thrust resolves a number of issues in the kinematics of deformation in the western margin of the Yakutat collisional system. In the Tysdale et al. (1976b) interpretation of the structure as a normal fault, or gravitational slide, the RMF would have to be kinematically disconnected from the regional deformation. With recognition the structure is a thrust, however, the RMF is wholly compatible with observed active deformation. In particular, the recognition of active thrusting with an increasingly oblique motion from south to north is compatible with interpretations by Bruhn et al. (2004) and Pavlis et al. (2014) that the RMF is the western limb of a large vertical axis fold in the suture. That is, accommodation of a large vertical axis fold would require both a component of shortening along an ENE axis but also a component of dextral shear to accommodate the folding; both consistent with the inferred kinematics.

Perhaps more importantly, however, the recognition that the RMF is indeed a thrust provides a broader perspective on the suturing process that accompanied the Yakutat collision. Geodynamic models of collision of indentors like the Yakutat microplate (e.g. Koons et al., 2010) indicate the margins of the indentor are marked by zones of opposite vorticity. In the specific case of the Yakutat collision, these models would predict a counterclockwise vorticity which should be manifest as a combination of vertical axis rotation and distributed sinistral shear along an axis sub-parallel to plate motion. The interpretation of the geometry of the suture is consistent with vertical axis rotation, and contraction along the NS-trending RMF is fully consistent with sinistral shear along NNW trending axis.

6 Conclusions

Our paleoseismic trenches indicate that the number and timing of the latest three ruptures on the antislope scarp overlap with those on the thrust scarp, permitting a mechanical connection between the two. The preferred structural model calls for an abrupt flattening of the thrust beneath the range front toe, which creates a collapsed thrust tip and a zone of secondary, antislope normal faults. Antislope scarp ruptures date at 0.5-3.9 ka; slightly younger than 8.3 ka; and 18.1-21.8 ka (recurrence intervals 4.4-8 kyr and 9.8-13.3 kyr). Displacements per event range from 15 to 40 cm. In the thrust trench ruptures date at 2.8-5.9 ka; 5.9-17.2 ka, and 17.2-44.9 ka (mean recurrence intervals 7.2 kyr and 19.5 kyr). Displacements per event ranged from 26-77 cm.The largest trench displacement (77 cm) equates to the average displacement expected for a 33 km-long reverse rupture (Wells and Coppersmith, 1994). Since the time of the

MRE (~4 to 5.8 ka) the flexural-slip scarp displays evidence of continuing synsedimentary tightening of the footwall syncline to the present. This may be interseismic deformation in ductile strata, or a delayed response to the 4.2 ka MRE. The southern third of the fault is dominated by large gravitational failures of the range front (as large as 2.5 km wide, 0.6-0.7 km long, and 200-250 m thick), which culminate in a linear, 40 m-deep range-crest trough filled with lakes, a classic expression of deep-seated gravitational slope deformation. The geomorphic and trench evidence provide a coherent picture of an active thrust fault system over the past ~20 ka, which is consistent with the plate tectonic setting, geodetic deformation, and earthquake focal mechanisms.

Acknowledgments

This work was performed as part of the Saint Elias Erosion and Tectonics Project (STEEP) supported through the NSF Continental Dynamics Program and Office of Polar Programs, with specific support from NSF grants EAR-0409009 and EAR-0735402 to Pavlis and EAR-0408959 to Bruhn.

References

Aitken, M.J. 1998. An Introduction to Optical Dating. Oxford Sci. Publ., 267pp.

Arrowsmith, R., Crosby, C., Korjenkov, A., Mamyrov, E., Povolotskaya, I., Guralnik, B., Landgraf, A. 2016. Surface rupture of the 1911 Kebin (Chon-Kemin) earthquake, Northern Tien Shan, Kyrgyzstan, In: Landgraf, A., Kübler, S., Hintersberger, E., Stein, S. (Eds.), Seismicity, Fault Rupture and Earthquake Hazards in Slowly Deforming Regions. Geol. Soc. London, Spec. Publ. 432, 233-254.

Audemard, F.A. 1999. Morpho-structural expression of active thrust fault systems in the humid tropical foothills of Colombia and Venezuela. Zeitschr. für Geomorphol. 118, 227-244.

Barrell, D.J.A. 2013. General distribution and characteristics of active faults and folds in the Selwyn District, North Canterbury (New Zealand). GNS Science Consultancy Report, Report No. R13/27, ISBN 978-1-927234-79-2, 53 p.

Briner, J.P., Kaufman, D.S., Manley, W.F., Finkel, R.C., Caffee, M.W. 2005. Cosmogenic exposure dating of late Pleistocene moraines stabilization in Alaska. Geol. Soc. Amer. Bull. 117(7-8), 1108-1120.

Briggs, R.W., Wesnousky, S.G. 2005. Late Pleistocene and Holocene paleoearthquake activity of the Olinghouse Fault Zone, Nevada. Bull. Seism. Soc. Amer. 95(4), 1301-1313.

Bruhn, R.L., Pavlis, T.L., Plafker, G., Serpa, L. 2004. Deformation during terrane accretion in the Saint Elias orogen, Alaska. Geol. Soc. Amer. Bull. 117(7), 771-787.

Bruhn, R.L., Sauber, J., Cotton, M.M., Pavlis, T.L., Burgess, E., Ruppert, N., Forster, R.R. 2012. Plate margin deformation and active tectonics along the northern edge of the Yakutat Terrane in the Saint Elias Orogen, Alaska, and Yukon, Canada. Geosphere 8(6), 1384-1407.

Chapman, J.B., Pavlis, T.L., Gulick, S., Berger, A., Lowe, L., Spotila, J., Bruhn, R., Vorkink, M., Koons, P., Barker, A., Picornell, C., Ridgway, K., Hallet, B., Jaeger, J., McCalpin, J. 2008. Neotectonics of the

Yakutat collision; Changes in deformation driven by mass redistribution, In: Freymueller, J.T., Haeussler, P.J., Wesson, R.L, Ekstrom, G. (Eds.), Active Tectonics and Seismic Potential of Alaska. Amer. Geophys Union, Monograph 179, 65-82.

Clark, K.J., Litchfield, N.J., Bartholomew, T., Van Dissen, R.J., Little, T.A. 2011. The Vernon Fault: Onshore paleoseismicity, constraints on slip rate, and contribution to Holocene tectonic subsidence of Big Lagoon, South Island, New Zealand. GNS Science Report 2011/42, Lower Hutt, New Zealand, 37 p.

Cotton, C. A. 1950. Tectonic scarps and fault valleys. Geol. Soc. Amer. Bulletin 61, 717—758.

Crook, R. Jr., Allen, C.R., Kamb, B., Payne, C.M., Proctor, R.J. 1987. Quaternary geology and seismic hazard of the Sierra Madre and associated faults, western San Gabriel Mountains: Chapter 2 in Recent Reverse Faulting in the Transverse Ranges, California, U.S. Geol. Survey Professional Paper 1339, 27-64.

Dart, C., Cohen, H.A., Aykuz, H.S. , Barka, A. 1995. Basinward migration of rift-border faults; implications for facies distributions and preservation potential. Geol. 23(1), 69-72.

Elliott, J., Freymueller, J.T., Larsen, C.F. 2013. Active tectonics of the St. Elias orogen, Alaska, observed with GPS measurements. Jour. Geophys. Res.118, 5625-5642.

Eusden, J.D., Pettinga, J.R. , Campbell, J.K. 2005. Structural collapse of a transpressive hanging-wall fault wedge, Charwell region of the Hope fault, South Island, New Zealand. New Zealand Jour. Geol. & Geophys. 48(2), 295-309.

Fraser, J., Pigati, J.S., Hubert-Ferrari, A., Vanneste, K., Avsar, U., Altinok, S. 2009. A 3000-year record of ground-rupturing earthquakes along the central North Anatolian Fault near Lake Ladik, Turkey. Bull. Seismol. Soc. Amer. 99(5), 2681-2703.

Freymueller, J.T., Woodard, H., Cohen, S.C., Cross, R., Elliott, J., Larsen, C.F., Hreinsdottir, S., Zweck, C. 2008. Active deformation processes in Alaska, based on 15 years of GPS measurements, In: Freymueller, J.T., Haeussler, P.J., Wesson, R.L., Ekstrom, G. (Eds.), Active Tectonics and Seismic Potential of Alaska. Amer. Geophys. Union, Geophys. Mon. 179, 23-65.

Gutiérrez, F., Carbonel, D., Kirkham, R.M., Guerrero, J., Lucha, P., Matthews, V. 2014. Can flexural-slip faults related to evaporite dissolution generate hazardous earthquakes? The case of the Grand Hogback monocline of west-central Colorado. Geol. Soc. Amer. Bull. 126, 1481-1494.

Heinlein, S.N., Pavlis, T.L. and Bruhn, R.L. in press. LiDAR DEM and high resolution aerial photography provides new insight into the role of tectonics versus gravitational deformation to resolve surface structure – Ragged Mountain, Katalla, Alaska, USA. Geosphere (in press).

Kachadoorian, R. 1956. Engineering geology of the Katalla area, Alaska. U.S. Geol. Surv. Open-File Report 56-66, 21 p., 4 maps at 1:40,000 scale.

Kelsey, H.M., Sherrod, B.L., Nelson, A.R., Brocher, T.M. 2008. Earthquakes generated from bedding plane parallel reverse faults above an active wedge thrust, Seattle fault zone. Geol. Soc. Amer. Bull. 120, 1581-1597.

Koehler, R.D. 2013. Quaternary faults and folds (QFF). Alaska Division of Geol.& Geophys. Surveys, Digital Data Series 3, http://doi.org/10.14509/qff.

Koons, P.O., Hooks, B.P., Pavlis, T., Upton, P., Barker, A.D. 2010. Three-dimensional mechanics of Yakutat convergence in the southern Alaska plate corner. Tectonics29, TC4008, doi:10.1029/2009TC002463.

Langridge, R.M., Berryman, K.R. 2005. Morphology and slip rate of the Hurunui section of the Hope Fault, South Island, New Zealand. New Zealand Jour. Geol. & Geophys. 48(1), 43-57.

Li, X., Huang, W., Pierce, I.K.D., Angster, S.J., Wesnousky, S.G. 2017. Characterizing the Quaternary expression of active faulting along the Olinghouse, Carson, and Wabuska lineaments of the Walker Lane. Geosphere 13(6), 2119–2136.

Li, Z., Bruhn, R.L., Pavlis, T.L., Vorkink, M., Zeng, Z. 2010. Origin of sackung uphill-facing scarps in the Saint Elias orogen, Alaska: LIDAR data visualization and stress modeling. Geol. Soc. Amer. Bull.122, 1585-1599.

Litchfield, N.J. and 48 others 2018. Surface rupture of multiple crustal faults in the 2016 Mw 7.8 Kaikoura, New Zealand, Earthquake. Bull. Seism. Soc. Amer. 108(3B), 1496-1520.

Mann, P., Burke, K., Matumoto, T. 1984. Neotectonics of Hispaniola: plate motion, sedimentation, andseismicity at a restraining bend. Earth. Plan. Sci. Lett. 70, 311-324.

Mackenzie, D., Elliott, A. 2017. Untangling tectonic slip from the potentially misleading effects of landform geometry. Geosphere 13(4), 1310-1328.

Mattahuer, M. 1973. Les deformations des matériaux de l'écorceterrestre. Hermann, Paris, 493 pp.

McCalpin, J.P. 1996. Tectonic geomorphology and Holocene paleoseismicity of the Molesworth section of the Awatere Fault, South Island, New Zealand. New Zealand Jour. Geol. & Geophys. 39(1), 33-50.

McCalpin, J.P. , Carver, G.A. 2009. Paleoseismology in compressional environments, In: McCalpin, J.P. (Ed.), Paleoseismology, 2nd Edition. Academic Press, New York, 317-420.

McCalpin, J.P., Bruhn, R.L., Pavlis, T.L., Gutierrez, F., Guerrero, J., Lucha, P. 2011. Antislope scarps, gravitational spreading, and tectonic faulting in the western Yakutat microplate, south coastal Alaska. Geosphere 7, 1143-1158.

McClay, K.R.1992. Glossary of thrust tectonics terms, In: McClay, K.R. (Ed.), Thrust Tectonics. Chapman and Hall, London, 419-447.

Morell ,K.D., Regalla, C., Leonard, L.J., Amos, C., Levson, V. 2017. Quaternary rupture of a crustal fault beneath Victoria, British Columbia, Canada. Geol. Soc. Amer., GSA Today 27(3), 4-10.

Murray, A.S., Wintle, A.G. 2000. Luminescence dating of quartz using an improved single aliquot regenerative-dose protocol. Radiation Meas. 32, 57-73.

Murray, A.S., Wintle, A.G. 2003. The single aliquot regenerative dose protocol: potential for improvements in reliability. Radiation Meas. 37, 377-381.

Pavlis, T.L., Enkelmann, E., Gulick, S.P.S., Pavlis, G. 2014. Introduction: Neogene tectonics and climate-tectonic interactions in the southern Alaska orogen themed issue: Geosphere, 10 (3), 424-427.

Philip, H., Meghraoui, M. 1983. Structural analysis and interpretation of the surface deformations of the El Asnam earthquake of October 10, 1980. Tectonics 2, 17–49.

Plafker, G. 1987. Regional geology and petroleum potential of the northern Gulf of Alaska continental margin, In: Scholl, D.W., Grantz, A. and Vedder, J.G. (Eds.), Geology and resource potential of the continental margin of western North America and adjacent ocean basins; Beaufort Sea to Baja California. Circum-Pacific Council for Energy and Mineral Resources, Earth Science Series, Houston, 229-268.

Prescott, J. R., Hutton, J.T. 1994. Cosmic ray contributions to dose rates for luminescence and ESR dating. Radiation Meas. 23, 497-500.

Rittenour, T.M., Goble, R.J., Blum, M.D. 2003. An optical age chronology of fluvial deposits in the northern Lower Mississippi Valley. Quat. Sci. Rev. 22, 1105-1110.

Rittenour, T.M., Goble, R.J., Blum, M.D. 2005. Development of an OSL chronology for late Pleistocene channel belts in the lower Mississippi valley. Quat. Sci. Rev.24, 2539-2554.

Schermer , E.R., Van Dissen , R., Berryman, K.R., Kelsey, H.M., Cashman, S.M. 2004. Active faults, paleoseismology, and historical fault rupture in northern Wairarapa, North Island, New Zealand. New Zealand Jour. Geol. & Geophys. 47(1), 101-122.

Shah, H.C., Bertero, V. (Cords.) 1980. El-Asnam earthquake, Algeria, 10th October 1980. Preliminary Reconnaissance Report. Earthquake Engr. Res. Inst., Berkeley, Calif., 64 p.

Strom, A., Abdrakhmatov, K., Djumabaeva, A., 2015. Formation of upslope-facing normal fault scarps in the compressional neotectonics environment. Proc. of Int. Assoc Geomorph. Regional Conf., Barnaul, Russia, July 2-4, 2015, extended abstract, 96-100.

Tibaldi, A., Corrazato, C., Rust, D., Bonali, F.L., Pasquare Marioto, F.A., Korzhenkov, A.M., Oppizzi, P., Bonzanigo, L. 2015. Tectonic and gravity induced deformation along the active Talas-Fergana fault, Tien Shan, Kyrgystan:.Tectonophys. 657, 38-62.

Tuthill, S.J., Laird, W.M. 1966. Geomorphic effects of the earthquake of March 27, 1964, in the Martin – Bering rivers area, Alaska: U.S. Geol. Surv. Professional Paper 543-B, 29 p.

Tysdal, R.G., Hudson, T., Plafker, G. 1976a, Geologic map of the Cordova B-2 quadrangle and northern part of the Cordova A-2 quadrangle, south-central Alaska. U.S. Geol. Surv. Misc. Field Studies Map MF-783, scale 1: 63.360, 1 sheet.

Tysdal, R.G., Hudson, T., Plafker, G. 1976b. Surface features and recent movement along the Ragged Mountain fault, south-central Alaska. U.S. Geol. Surv. Misc. Field Studies Map MF-782, scale 1: 24,000, 1 sheet.

van Dissen, R. , Nicol, A. 2009. Mid-late Holocene paleoseismicity of the eastern Clarence Fault, Marlborough, New Zealand. New Zealand Jour. Geol. & Geophys. 52(3), 195-208.

Wesnousky, S.G. 2005. Active faulting in the Walker Lane. Tectonics 24(3), TC3009, doi:10.1029/2004TC001645.

Winkler, G.R., Plafker, G. 1993. Geologic map of the Cordova and Middleton Island quadrangles, southern Alaska. U.S. Geol. Surv. Map I-1984, scale 1:250,000.

Wintle, A.G. Murray, A.S. 2006. A review of quartz optically stimulated luminescence characteristics and their relevance in single-aliquot regenerative protocols. Radiation Meas. 41, 369-391.

SUPPLEMENTS

Supplementary Figure 1

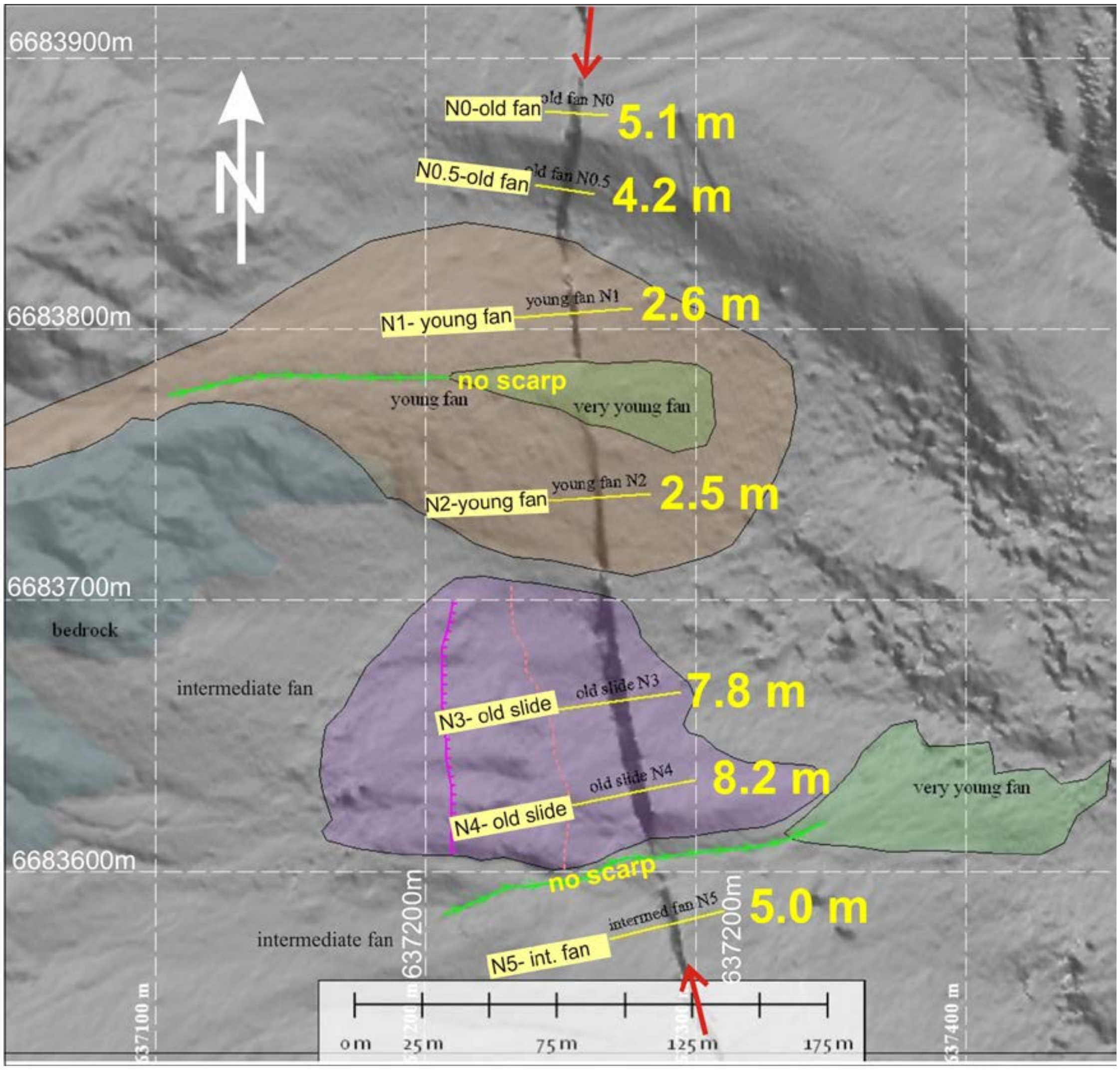

Figure S1. Surficial geologic map and vertical separations (yellow; graphically estimated from transverse topographic profiles) across the antislope scarp (dark band between red arrows) in the southernmost part of the North Central sub-section. In this lidar hillshade illumination is from N45°E, so the west-facing scarp face makes a dark shadowed band which is wider on the higher scarps. Hummocky topography downslope of the fans reflects large boulders from rockfalls.

Supplementary Figure 2

Figure S2. Panorama of large rockfall deposit containing big blocks and displaced at the antislope scarp. View is to SSE from 637262mE, 6683740mN, NAD83. There are no anomalously large blocks caught by the scarp, which suggests that the scarp formed after the large rockfall. Subsequently, a small wedge-shaped deposit of younger talus has accumulated against the scarp.

Fig. S2 shows typical interactions between the rockfall deposits and the antislope scarp. The camera position is on scarp profile “N2-young fan” shown on Fig. S1. At far left the largest rockfall boulders and thickest deposit are at and below the slope break on the footwall bench (the accumulation zone). Rockfall deposits thin upslope (in the transport zone) and are <1 m thick at the antislope scarp. The large snowfield at far right fills the graben mentioned previously at profiles “N3- and N4-old slide.” The bottom of the 10 m-high, dissected, valley-facing scarp mapped on Figs. 8 and S1 is visible just upslope of the snowfield.

Supplementary Figure 3

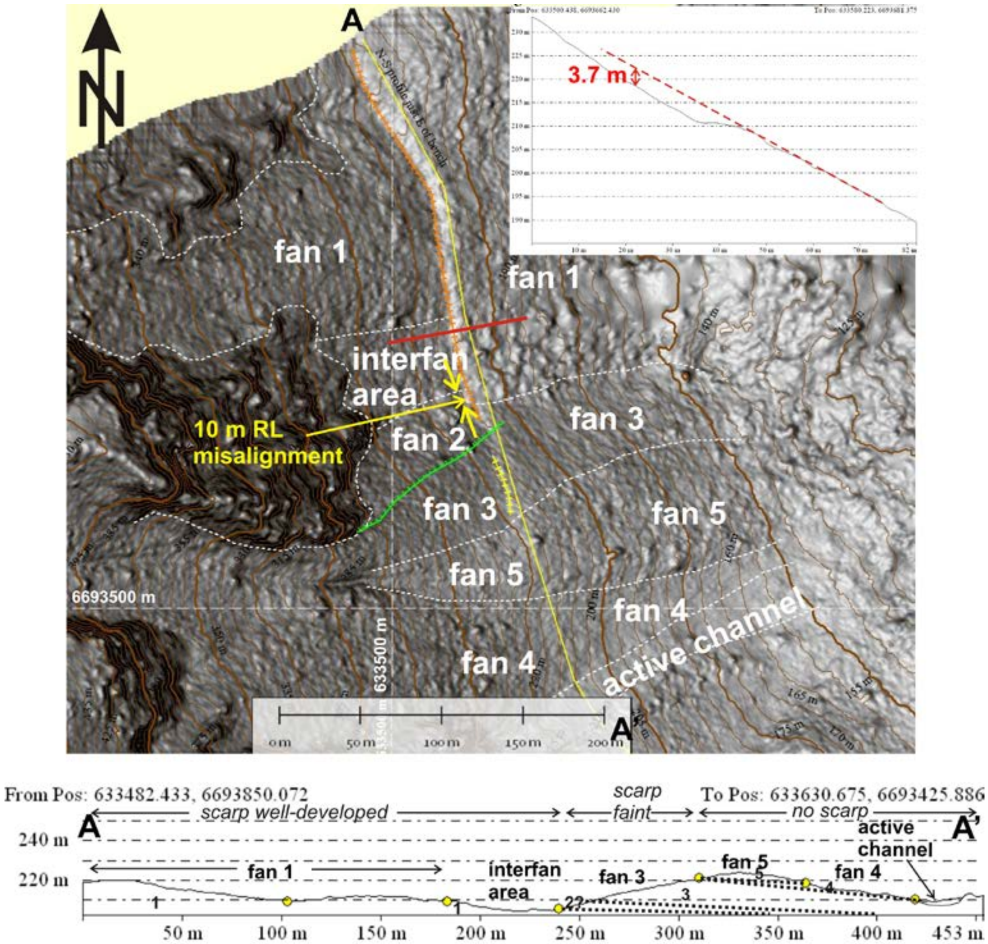

Figure S3. Annotated lidar slopeshade of the northern end of the antislope "scarp" of the RMF. Scarp is actually a bench here (white band at upper center, see Inset at upper right). There is no scarp on the younger surfaces (active channel, fan 5, and fan 4). Scarp is faint across fan 3, better developed across fan 2, and best developed across fan 1, where the vertical separation across the bench is 3.7 m. The inferred geometry of the faulted and unfaulted fan deposits is shown by longitudinal section A-A' at bottom (line of section shown by a thin yellow line on map).

Supplementary Figure 4

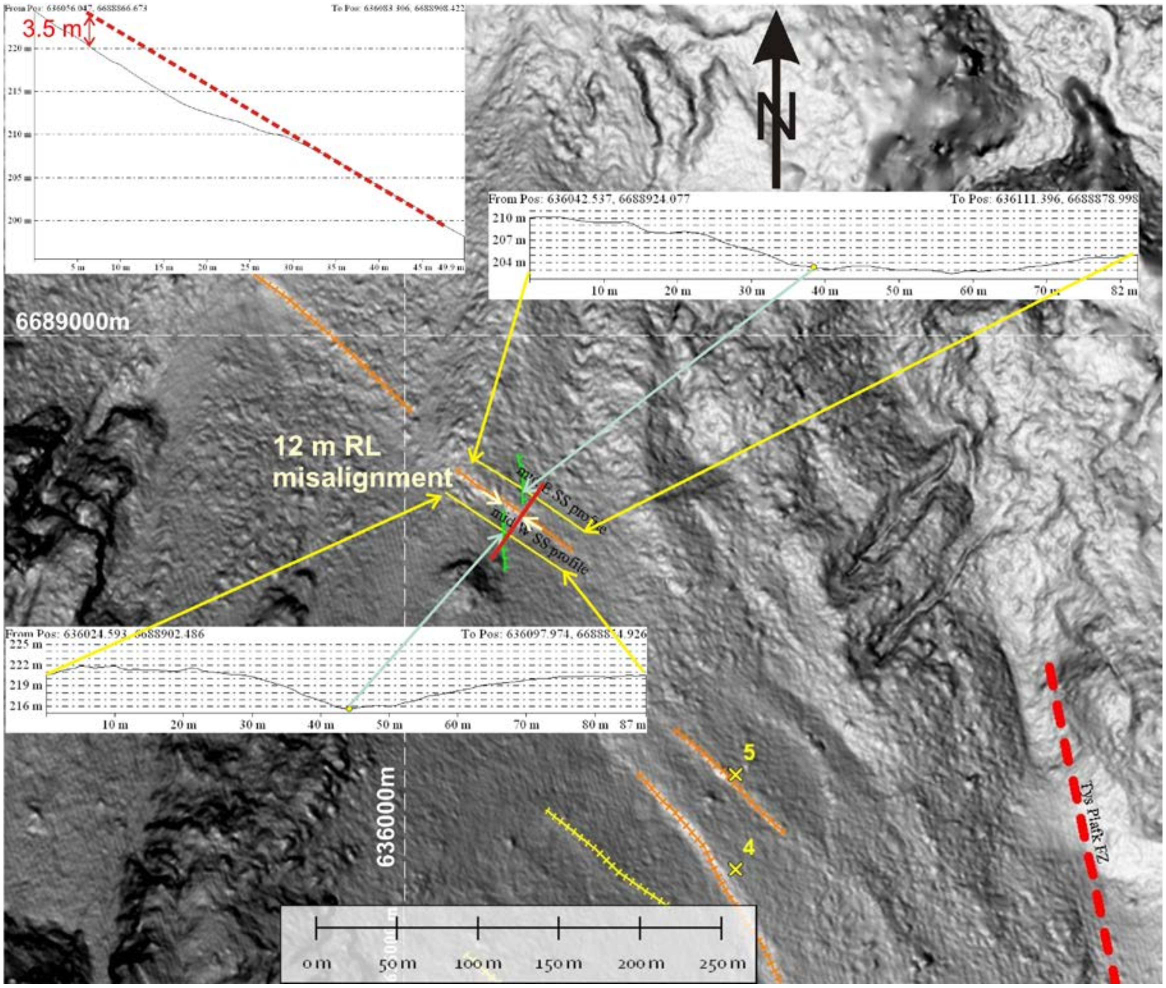

Figure S4. Annotated lidar slopeshade of the southern end of the antislope "scarp" of the RMF. Scarp is a gently-sloping bench here (white band at upper center, see Inset at upper left). There is no scarp on the younger surfaces (active channel, fan 5, and fan 4). Scarp is faint across fan 3, better developed across fan 2, and best developed across fan 1, where the vertical separation across the bench is 3.7 m. The inferred geometry of the faulted and unfaulted fan deposits is shown by longitudinal section A-A' at bottom (line of section shown by a thin yellow line on map).

Supplementary Figure 5

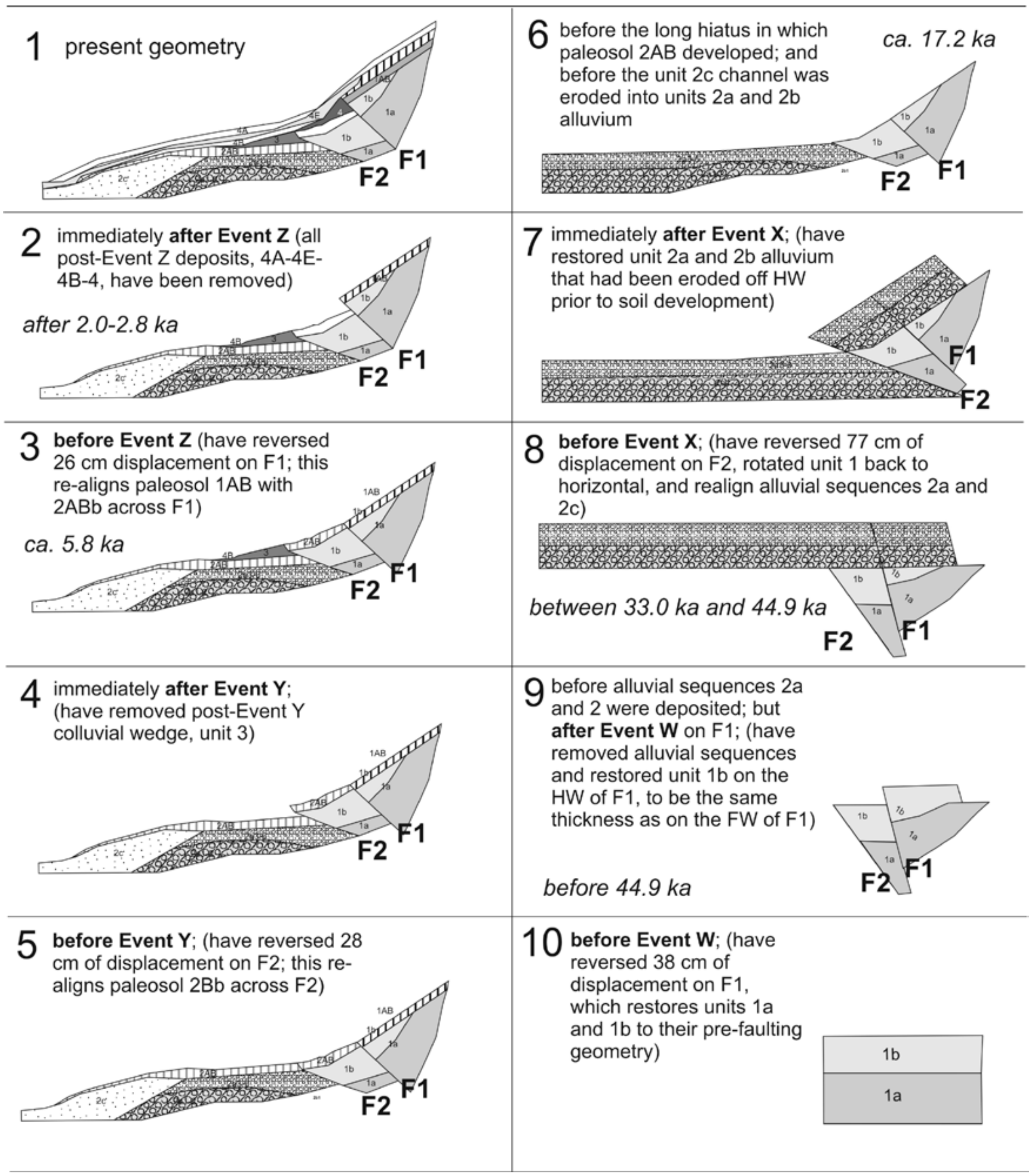

Fig. S5. Retrodeformation sequence of Trench 4. Stage 1 is present geometry, Stage 10 is pre-faulting geometry. Each Stage lists appropriate OSL ages, and the changes made to the previous stage diagram. The geometry of Stages 1-5 is well constrained, but Stages 6-10 are more speculative, due to erosional removal of stratigraphy on the uplifted hanging-wall fault blocks.

Supplementary Figure 6

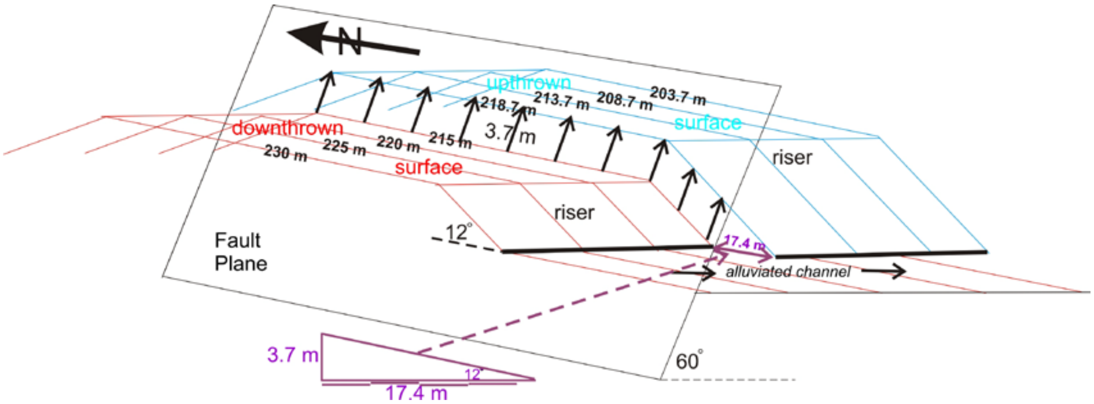

Figure S6. Simplified wireframe diagram of an east-sloping alluvial fan with steepened lateral margins, displaced 3.7 m vertically by a North-trending antislope scarp (thick arrows). Lines on the upthrown and downthrown surfaces are contour lines. The 3.7 m vertical uplift, and predicted RL misalignment of the margin toe (thick black line) by 17.4 m (purple arrow), are exaggerated for clarity. The matching LL misalignment of the left-side margin is not shown.

Supplementary Figure 7

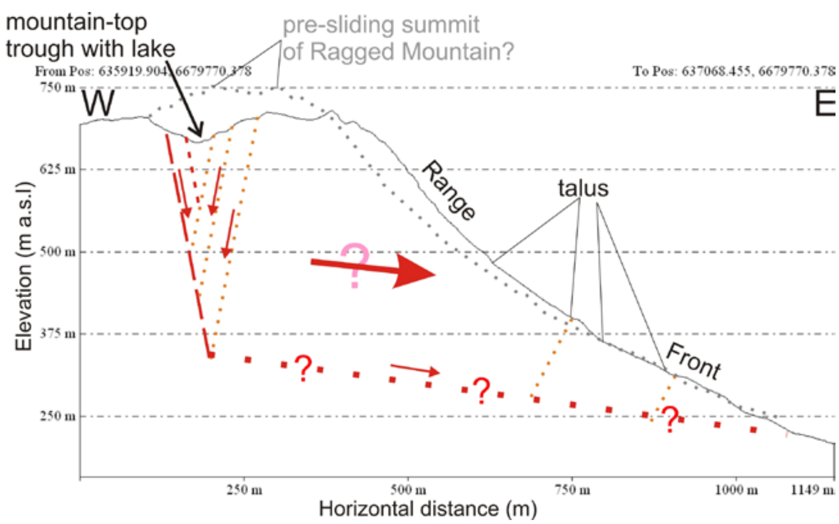

Figure S7. West-to-east topographic profile through the summit and range front of Ragged Mountain in the northern part of the South Section (UTM coordinates of line ends appear after "From" and "To" at top of drawing). Subsurface structures and pre-sliding topography are speculative.

Supplementary Figure 8

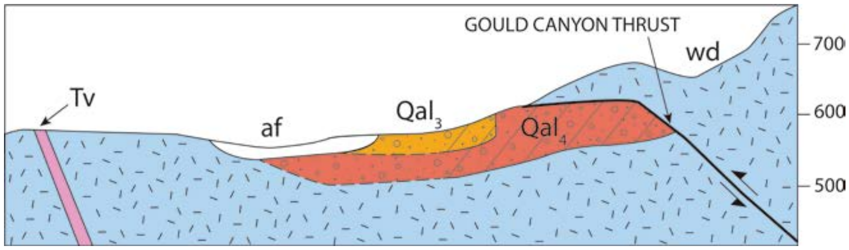

Figure S8. Cross-section showing a “thrust-rooted slide” (blue over red); North is at right. The Gould Canyon thrust (far right) places the Wilson Diorite (Cretaceous; in blue) over Quaternary alluvium (older Qal4 alluvium in red, younger Qal3 alluvium in orange). Note how the leading edge of the thrust has “rolled over” from a dip of 45°N (to the right) to a dip of 5°S over the alluvium. The diorite directly overlying the alluvium forms the landslide mass, which is about 250 m long; the scalloped-out area near the label “wd” farther upslope is the evacuated slide source area. Redrawn from Plate 2 in Crook et al. (1987).